AD-A057 504 AIRESEARCH MFG CO OF ARIZONA PHOENIX F/G 20/4
TRANSONIC 3-D FLOW ANALYSIS OF COMPRESSOR CASCADE WITH SPLITTER--ETC(U)
MAY 78 P R DODGE, L S LIEBER F33615-76-C-2071
UNCLASSIFIED 21-2524(3) AFAPL-TR-78-23 NL

1 OF 1
AD A057 504

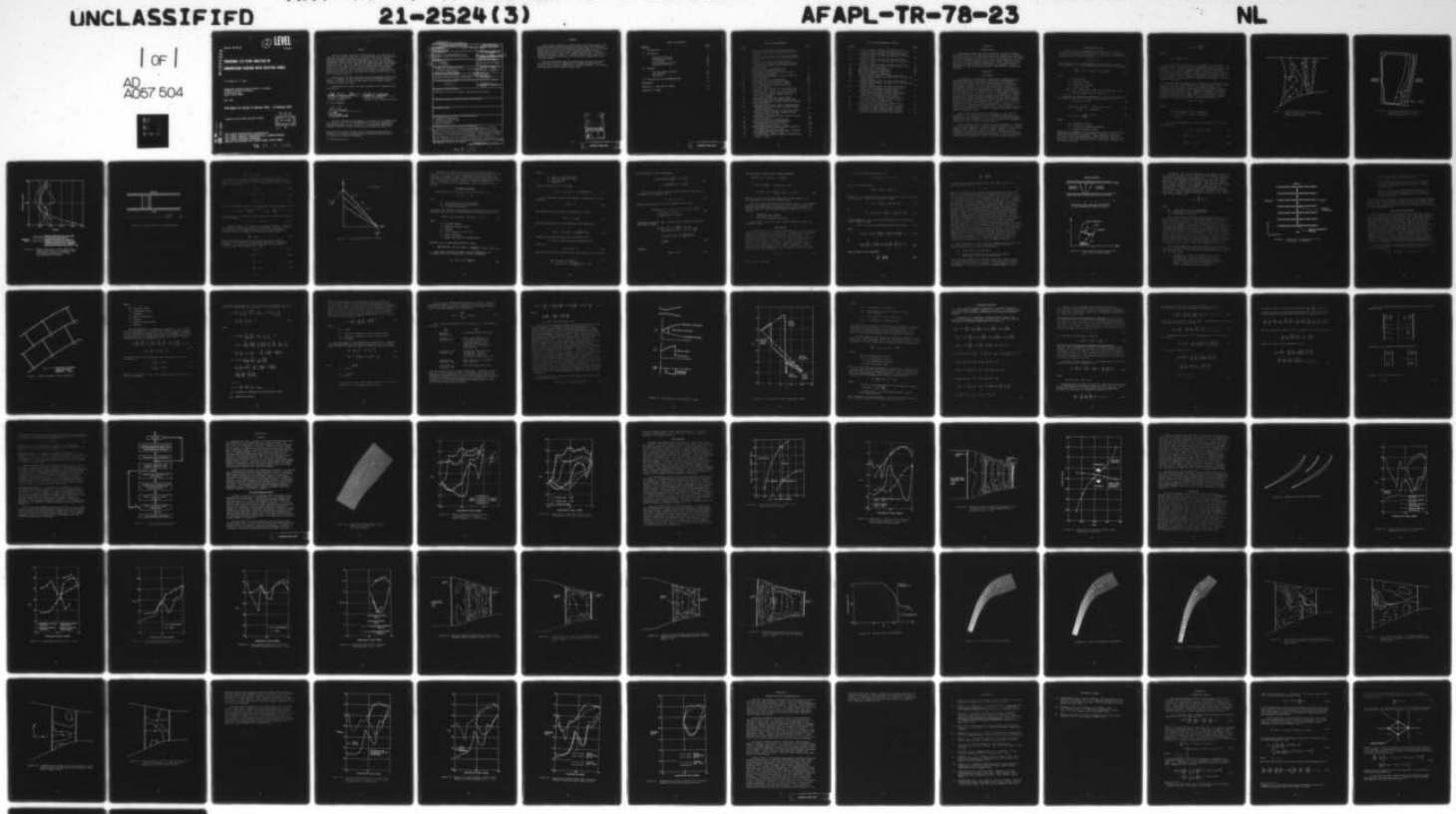

END
DATE FILMED
9-78
DDC

(2) LEVEL II

AFAPL-TR-78-23

21-2524(3)

AD A057504

TRANSONIC 3-D FLOW ANALYSIS OF COMPRESSOR CASCADE WITH SPLITTER VANES

P. R. Dodge and L. S. Lieber

AIRESEARCH MANUFACTURING COMPANY OF ARIZONA
A Division of The Garrett Corporation
111 South 34th Street
Phoenix, Arizona 85034

MAY 1978

Final Report for Period 13 February 1976 – 13 February 1978

Approved for public release; distribution unlimited.

AIR FORCE PROPULSION LABORATORY
AIR FORCE WRIGHT AERONAUTICAL LABORATORIES
AIR FORCE SYSTEMS COMMAND
WRIGHT-PATTERSON AIR FORCE BASE, OHIO 45433

NOTICE

When Government drawings, specifications, or other data are used for any purpose other than in connection with a definitely related Government procurement operation, the United States Government thereby incurs no responsibility nor any obligation whatsoever; and the fact that the government may have formulated, furnished, or in any way supplied the said drawings, specifications, or other data, is not to be regarded by implication or otherwise as in any manner licensing the holder or any other person or coporation, or conveying any rights or permission to manufacture, use, or sell any patented invention that may in any way be related thereto.

This report has been reviewed by the Information Office (OI) and is releasable to the National Technical Information Service (NTIS). At NTIS, it will be available to the general public, including foreign nations.

This technical report has been reviewed and is approved for publication.

Arthur J. Wennerstrom
ARTHUR J. WENNERSTROM
Project Engineer

Walter H. Mitchell
WALKER H. MITCHELL
Acting Chief, Technology Branch

For the Commander

H. I. Bush
H. I. BUSH
Deputy Director
Turbine Engine Division

"If your address has changed, if you wish to be removed from our mailing list, or if the addressee is no longer employed by your organization please notify A. J. Wennerstrom (AFAPL/TBX), W-PAFB, OH 45433 to help us maintain a current mailing lift".

Copies of this report should not be returned unless return is required by security considerations, contractual obligations, or notice on a specific document.

AIR FORCE/56780/14 July 1978 — 200

Unclassified

SECURITY CLASSIFICATION OF THIS PAGE (When Data Entered)

REPORT DOCUMENTATION PAGE	READ INSTRUCTIONS BEFORE COMPLETING FORM
1. REPORT NUMBER: AFAPL-TR-78-23	2. GOVT ACCESSION NO. / 3. RECIPIENT'S CATALOG NUMBER
4. TITLE (and Subtitle): TRANSONIC 3-D FLOW ANALYSIS OF COMPRESSOR CASCADE WITH SPLITTER VANES	5. TYPE OF REPORT & PERIOD COVERED: Final Report, 13 Feb 76 - Feb 78
	6. PERFORMING ORG. REPORT NUMBER: 21-2524(3)
7. AUTHOR(s): P. R. Dodge, L. S. Lieber	8. CONTRACT OR GRANT NUMBER(s): F33615-76-C-2071
9. PERFORMING ORGANIZATION NAME AND ADDRESS: AiResearch Manufacturing Co. of Arizona, 111 South 34th Street, Phoenix, Arizona 85034	10. PROGRAM ELEMENT, PROJECT, TASK AREA & WORK UNIT NUMBERS: 2307-57-28, 57
11. CONTROLLING OFFICE NAME AND ADDRESS: Air Force Aero Propulsion Laboratory (TBX), Wright-Patterson AF Base, Ohio 45433	12. REPORT DATE: May 1978
	13. NUMBER OF PAGES: 87
14. MONITORING AGENCY NAME & ADDRESS (if different from Controlling Office): 84 p.	15. SECURITY CLASS. (of this report): Unclassified
	15a. DECLASSIFICATION/DOWNGRADING SCHEDULE

16. DISTRIBUTION STATEMENT (of this Report)

Approved for public release; distribution unlimited.

17. DISTRIBUTION STATEMENT (of the abstract entered in Block 20, if different from Report)

18. SUPPLEMENTARY NOTES

19. KEY WORDS (Continue on reverse side if necessary and identify by block number)

Transonic Compressors
Transonic Viscous Flow
Three Dimensions
Splitter Vanes

20. ABSTRACT (Continue on reverse side if necessary and identify by block number)

AiResearch has been developing the technology to perform transonic analysis of compressors as performance with and without splitter vanes. This has generally followed five phases of development, proceeding from a single-bladed cascade to splittered cascades, and finally a fully-rotating compressor. The sections in this report describe the basic method (description of geometry, radial equilibrium, and relaxation portions) & comparison data.

DD FORM 1 JAN 73 1473 EDITION OF 1 NOV 65 IS OBSOLETE

Unclassified

SECURITY CLASSIFICATION OF THIS PAGE (When Data Entered)

404 776

PREFACE

This report describes a contractual effort performed by the AiResearch Manufacturing Company of Arizona for the Technology Branch (TBX) of the Turbine Engine Division (TB), Air Force Aero Propulsion Laboratory, Air Force Systems Command, Wright-Patterson Air Force Base, Ohio, under Project 2307, "Turbine Engine Technology", Task S1, "Turbine Technology", Work Unit 28, "Transonic Three-Dimensional Flow Analysis of Compressor with Splitter Vanes".

The work reported herein was performed during the period 13 February 1976 to 13 February 1978 under the direction of Arthur J. Wennerstrom (AFAPL/TBX), project engineer. The report was released by the authors in May 1978.

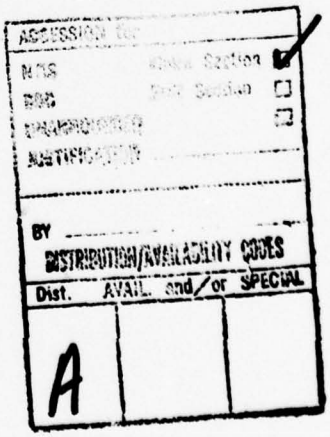

TABLE OF CONTENTS

LIST OF ILLUSTRATIONS

LIST OF ILLUSTRATIONS (CONTD.)

SECTION I

INTRODUCTION

AiResearch, under contract to USAF/APL (Contract Number F33615-76-C-2071), has been developing the technology to perform transonic analysis of compressors with and without splitter vanes. This has generally followed five phases of development, proceeding from a single-bladed cascade to splittered cascades, and finally to a fully-rotating compressor. The following sections describe the basic method (description of geometry, radial equilibrium, and relaxation portions) and present a comparison to data.

SECTION II

THE METHOD

By necessity, the design of transonic compressors has always been performed utilizing methods that are incapable of predicting the real flow fields internal to such devices. Consequently, there has been a heavy reliance on test-based development programs. The cost of testing has, however, increased so rapidly that the amount of testing, and therefore the performance of new components, is largely controlled by fiscal constraints. The bright spot, in what would otherwise be a gloomy outlook, is that the cost of computing has steadily declined as larger and larger computers are developed. This, coupled with vastly improved numerical methods, has resulted, for at least some turbomachinery devices, in the replacement of testing by computational experiments. However, of all turbomachinery devices, the transonic compressor is one of the most complicated. Computational developments for this device initially concentrated on transonic flow. Among these developments has been the work of Dodge[1,2] applying transonic relaxation to internal flows.

Rae[3,4] has applied similar techniques to the full 3-D compressor. The calculations were limited to extremely low-pressure-ratio compressors, due to the perturbation assumption utilized by Rae. Tompkins et al.[5] have applied time-dependent techniques to fully-rotating compressors.

More recently, Dodge's method has been extended to transonic fully-viscous solutions to stator systems having nearly irrotational vector diagrams. It would appear natural to extend this method to more general compressor cases. However, in the presence of large circulation gradients, difficulties confront the direct application of such an approach. The following sections outline a numerical method for these particular cases.

Equation Splitting

Dodge[6] described a successful technique of analyzing viscous flow in turbomachine stators. The basis of this technique is substituting a potential gradient plus a rotational component for the velocity vector.

$$\vec{W} = \nabla\phi + \vec{U} \tag{1}$$

When Equation (1) is substituted into the momentum Equation (2), the result is a split between potential and viscous terms.

$$\rho \frac{D\vec{W}}{Dt} = -\nabla P + \nabla(\lambda \nabla\cdot\vec{W}) + \nabla\cdot[\mu_e \, \mathrm{def}\vec{W}] \tag{2}$$

where

ρ = the density

$\vec{W}$ = velocity vector

μ_e = effective viscosity

P = static pressure

$\mathrm{def}\vec{W} = \nabla\vec{W} + (\nabla\vec{W})^*$ where $(\nabla\vec{W})^*$ is the transpose of $\nabla\vec{W}$

λ = second coefficient of viscosity

Pressure is related to potential, as given by Equation (3) for compressible flow, leaving a viscous Equation (4).

$$\rho^* \, \nabla\phi\cdot\nabla(\nabla\phi) = -\nabla P \tag{3}$$

$$\rho(\vec{W}\cdot\nabla)\,\vec{U} + \rho\vec{U}\cdot\nabla(\nabla\phi) - (\rho^*-\rho)\,[\nabla\phi\cdot\nabla(\nabla\phi)] = \nabla\,(\lambda\nabla\cdot\vec{W}) + \nabla\cdot\,[\mu_e \, \mathrm{def}\,\vec{W}] \tag{4}$$

$$\rho^* = \rho'_I \left(1 - \frac{\nabla\phi\cdot\nabla\phi}{2h'_I}\right)^{1/\gamma-1} \tag{5}$$

where

ρ'_I = reference density

h'_I = reference stagnation enthalpy

γ = ratio of specific heats

Equation (3) combined with an equation-of-state and the continuity equation yields an equation for potential, which is solved by transonic relaxation. Dodge indicates that such a splitting, with appropriate boundary conditions, results in an equation for which a potential vector satisfying Equation (6) can always be found.

$$P = P'_I \left(1 - \frac{\nabla\phi \cdot \nabla\phi}{2h'_I}\right)^{\gamma/\gamma-1} \tag{6}$$

where

$$P'_I = \left(\frac{\gamma-1}{\gamma}\right) \rho'_I \, h'_I$$

For cases involving little or no spanwise circulation gradients, excellent results are obtained by such a method. For example, Figure 1 shows the suction-surface static-pressure distribution on a high Mach number stator recently tested in a stage configuration by AFAPL. Figure 2 shows the distribution of loss at the exit. Figure 3 shows calculated radial-loss profiles compared to design and two different reductions of the measured data. The computations represent a reasonable representation of the data.

However, when applying such a technique to cases with large hub-to-shroud circulation variations, difficulties arise. For example, consider axial flow in a cylindrical duct with a constant axial velocity and no swirl in the absolute frame-of-reference (see Figure 4). No circulation gradient exists in the absolute reference frame. However, consider the rotating frame-of-reference that would occur. The vorticity in this frame-of-reference is 2ω where ω is the rotational frequency. Equation (7) gives the velocity vector for this case.

$$\vec{W} = \omega r \hat{\theta} + W_z \hat{z} \tag{7}$$

where

$\hat{\theta}$ = unit vector in the θ direction

$\hat{z}$ = unit vector in the z direction

r = radius

The potential component is given by Equation (8), yielding Equations (9).

$$\nabla\phi = \frac{\partial\phi}{\partial r} \hat{r} + \frac{1}{r} \frac{\partial\phi}{\partial\theta} \hat{\theta} + \frac{\partial\phi}{\partial z} \hat{z} \tag{8}$$

$$\frac{\partial\phi}{\partial r} + U_r = 0. \tag{9a}$$

$$\frac{1}{r} \frac{\partial\phi}{\partial\theta} + U_\theta = \omega r \tag{9b}$$

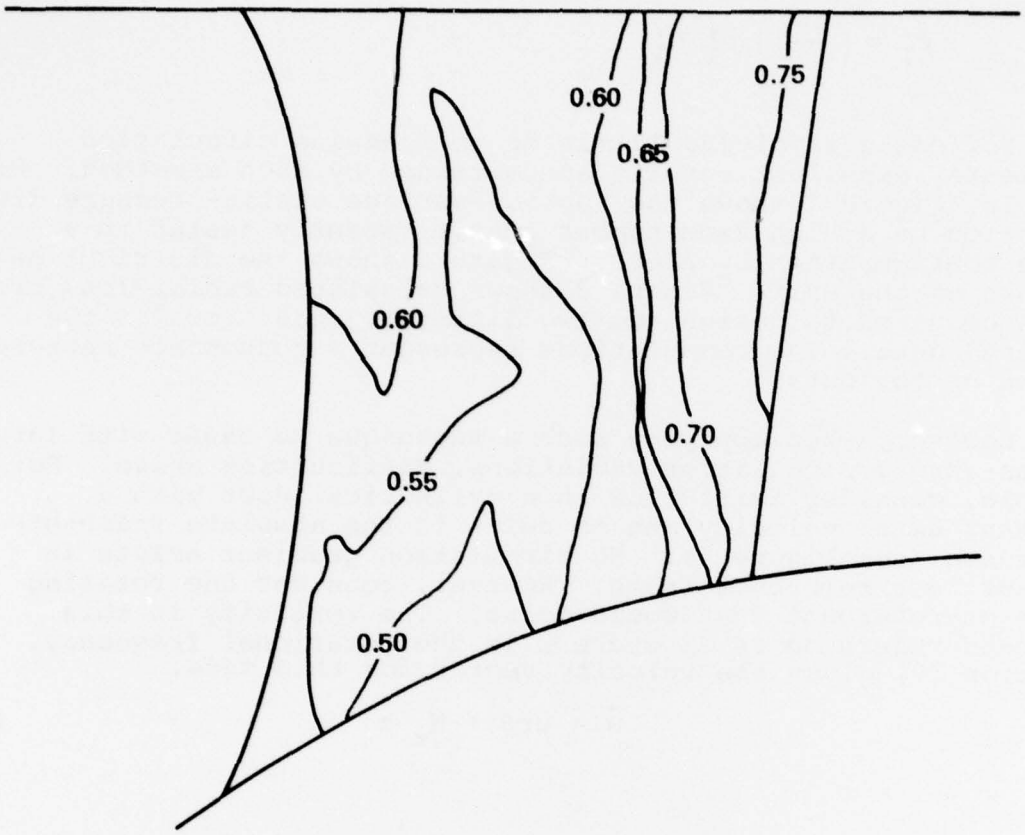

Figure 1. Suction Surface Lines of Constant Static Pressure Ratio for APL High-Through-Flow Stator

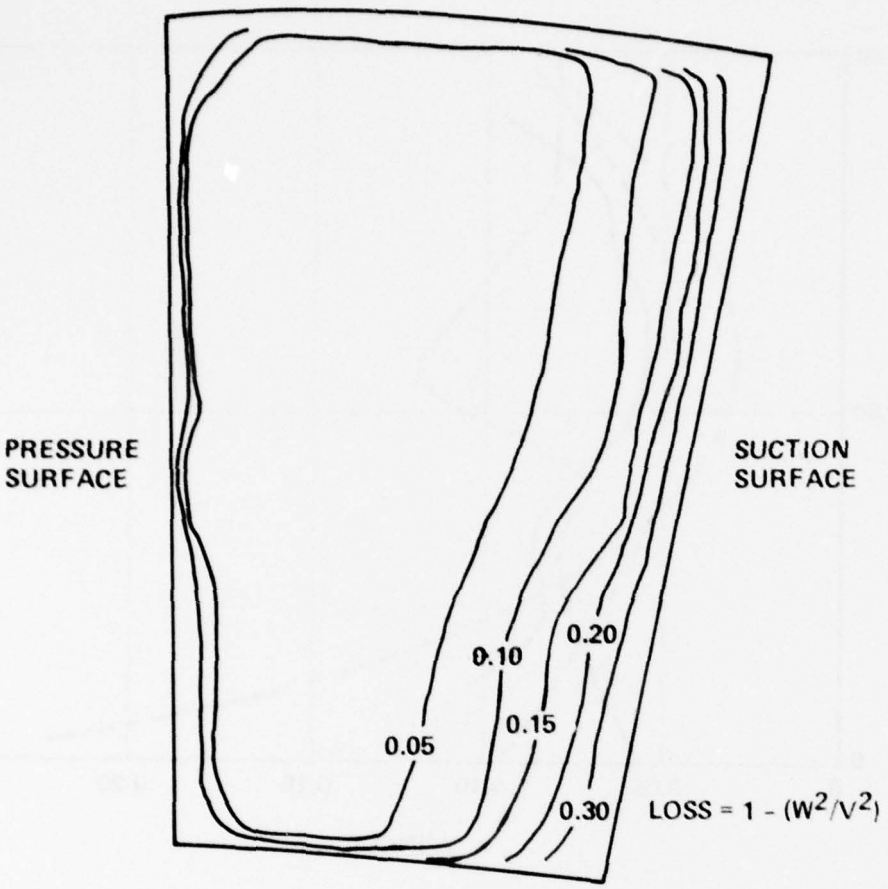

Figure 2. Lines of Constant Loss 0.6-Inch Downstream of Trailing Edge for APL High-Through-Flow Stator

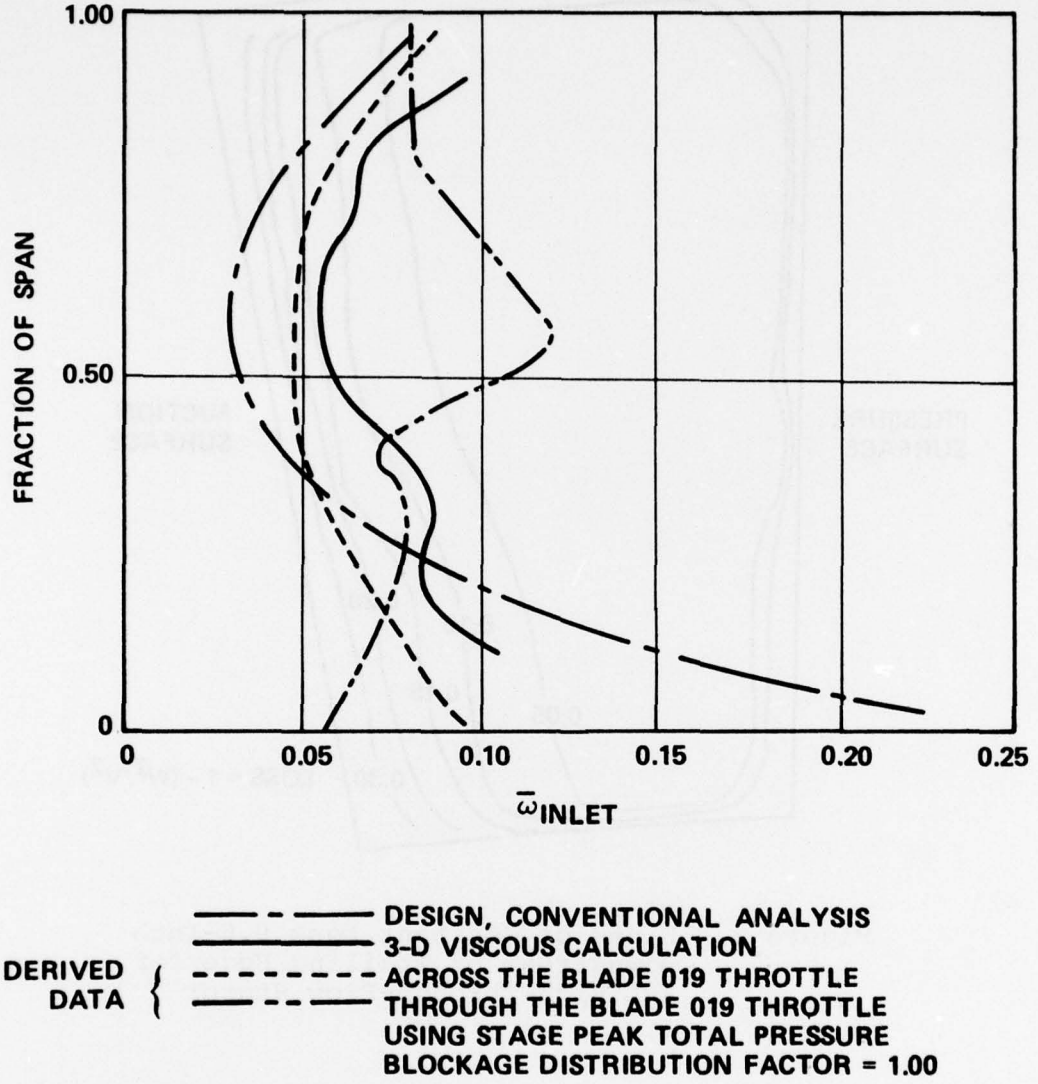

Figure 3. Radial Variation of Loss Coefficient -- Comparison of Design, Experiment and 3-D Viscous Calculation for APL High-Through-Flow Stator

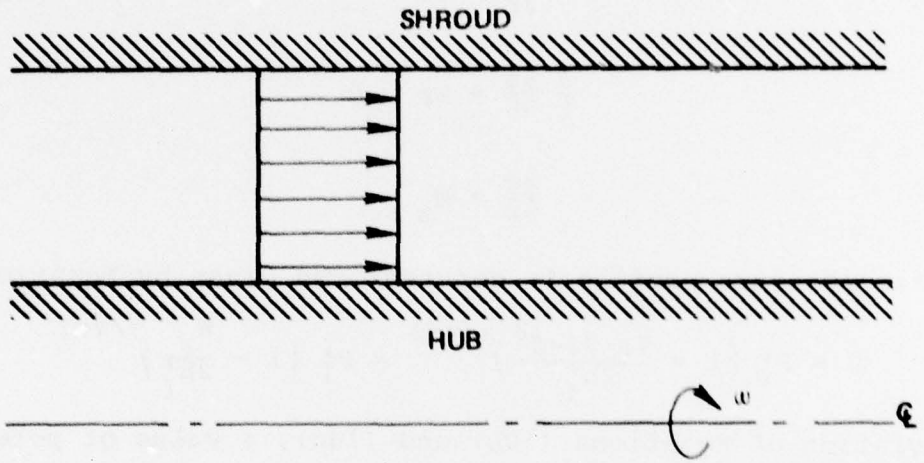

Figure 4. Axial Flow in a Cylindrical Duct

$$\frac{\partial \phi}{\partial z} + U_z = W_z \tag{9c}$$

One approach is to apply the inlet conditions of Dodge[6]. For this case, the rotational vector U must be identically zero resulting in Equations (10). It will be shown that these equations cannot be satisfied.

$$\frac{\partial \phi}{\partial r} = 0. \tag{10a}$$

$$\frac{1}{r}\frac{\partial \phi}{\partial \theta} = \omega r = C \tag{10b}$$

$$\frac{\partial \phi}{\partial z} = W_z \tag{10c}$$

The static pressure profile is constant, as given by Equation (11).

$$P = P_I' \left(1 - \frac{\nabla\phi \cdot \nabla\phi - C^2}{2h_I'}\right)^{\gamma/\gamma-1} = P_I' \left(1 - \frac{W_z^2}{2h_I'}\right)^{\gamma/\gamma-1} \tag{11}$$

By integration of Equations (10b) and (10c), a value of potential can be obtained.

$$\phi = \phi_o + W_z z + (\omega r)(r\theta) \tag{12}$$

Figure 5 shows a top view of a potential surface. Note that the potential surface is curved in the radial direction. Thus, the derivative of ϕ cannot be zero in the radial direction. Differentiation of Equation (12) yields the same result.

$$\frac{\partial \phi}{\partial r} = 2\omega r\theta \tag{13}$$

Thus, Equation (10a) can not be satisfied, and the static pressure is not constant in either the radial or θ direction. Therefore, to obtain a realistic solution, the rotational component must be contained in U. Thus:

$$U_\theta = \omega r \tag{14}$$

$$\frac{1}{r}\frac{\partial \phi}{\partial \theta} \equiv 0 \tag{15a}$$

$$\frac{\partial \phi}{\partial r} \equiv 0 \tag{15b}$$

$$\frac{\partial \phi}{\partial z} = W_z \tag{15c}$$

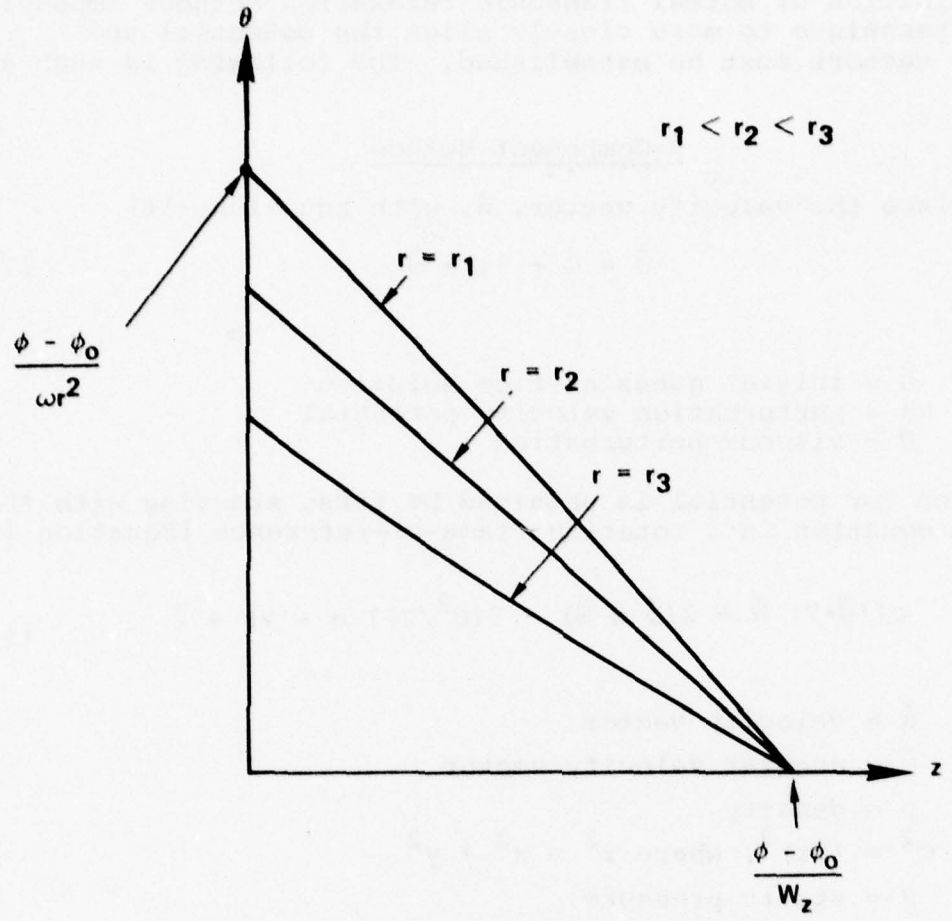

Figure 5. A Surface of Constant Potential

Equation (14) and Equations (15) meet the requirements, but the potential vector is severely misaligned from the velocity vector. For a typical axial compressor, the misalignment can approach 70 degrees. Such a consistent misalignment will make the application of normal transonic relaxation methods impossible. Thus, a technique to more closely align the potential and velocity vectors must be established. The following is such a method.

3-Component Method

Replace the velocity vector, $\vec{W}$, with Equation (16)

$$\vec{W} = \vec{G} + \nabla\phi + \vec{U} \tag{16}$$

where

$\vec{G}$ = initial guess at flow solution
$\nabla\phi$ = perturbation velocity potential
$\vec{U}$ = viscous perturbation

A solution for potential is obtained by first starting with the momentum equation in a rotating frame-of-reference (Equation 17).

$$\rho[(\vec{W}\cdot\nabla)\ \vec{W} + 2(\vec{\omega} \times \vec{W}) - \nabla(C^2/2)] = -\nabla P + \vec{\Sigma} \tag{17}$$

where

$\vec{W}$ = velocity vector
$\vec{\omega}$ = angular velocity vector
ρ = density
$C^2 = (\omega r)^2$, where $r^2 = x^2 + y^2$
P = static pressure
$\vec{\Sigma}$ = shear and Reynold's stress vector

Equation (17) is then dotted by $\vec{W}$ to yield

$$\rho\left\{\vec{W}\cdot[(\vec{W}\cdot\nabla)\vec{W}] + \vec{W}\cdot[2(\vec{\omega} \times \vec{W})] - \vec{W}\cdot\nabla\left(\frac{C^2}{2}\right)\right\} = -\vec{W}\cdot\nabla P + \vec{W}\cdot\vec{\Sigma} \tag{18}$$

The static pressure gradient may be expressed in the following form for an ideal gas (γ and R = constant).

$$\nabla P = a^2\nabla\rho + \rho a^2\left(\frac{\gamma-1}{\gamma R}\right)\nabla S \tag{19}$$

where

a = speed of sound (static)
γ = ratio of specific heats
R = gas constant
S = entropy

Dotting Equation (19) by $\vec{W}$ yields

$$\vec{W}\cdot\nabla P = a^2\ (\vec{W}\cdot\nabla\rho) + \rho a^2\left(\frac{\gamma-1}{\gamma R}\right)(\vec{W}\cdot\nabla S) \tag{20}$$

The continuity equation for steady, compressible flow is given by

$$\nabla\cdot(\rho\vec{W}) = 0 \tag{21}$$

or, expanding and rearranging Equation (21) gives

$$\vec{W}\cdot\nabla\rho = -\rho(\nabla\cdot\vec{W}) \tag{22}$$

Replacing Equation (22) into Equation (20) results in

$$\vec{W}\cdot\nabla P = -a^2\rho(\nabla\cdot\vec{W}) + \rho a^2\left(\frac{\gamma-1}{\gamma R}\right)\ (\vec{W}\cdot\nabla S) \tag{23}$$

Examining the cross-product term in Equation (18),

$\vec{\omega} \times \vec{W}$ is a vector normal to both $\vec{W}$ and $\vec{\omega}$.

Therefore,

$$\vec{W}\cdot(\vec{\omega} \times \vec{W}) = 0 \tag{24}$$

Substituting Equations (23) and (24) into Equation (18) yields

$$\rho\left\{\vec{W}\cdot[(\vec{W}\cdot\nabla)\vec{W}] - \vec{W}\cdot\nabla\left(\frac{C^2}{2}\right)\right\} = -\left[-a^2\rho(\nabla\cdot\vec{W}) + \rho a^2\left(\frac{\gamma-1}{\gamma R}\right)(\vec{W}\cdot\nabla S)\right] + \vec{W}\cdot\vec{\Sigma} \tag{25}$$

or dividing by ρ, and rearranging

$$\vec{W}\cdot[(\vec{W}\cdot\nabla)\vec{W}] - \vec{W}\cdot\nabla\left(\frac{C^2}{2}\right) - a^2\ (\nabla\cdot\vec{W}) = -a^2\left(\frac{\gamma-1}{\gamma R}\right)(\vec{W}\cdot\nabla S) + \frac{1}{\rho}\ (\vec{W}\cdot\vec{\Sigma}) \tag{26}$$

The velocity vector, $\vec{W}$, may then be separated into three components as in Equation (16)

$$\vec{W} = \vec{G} + \nabla\phi + \vec{U} \tag{27}$$

Substituting Equation (27) into Equation (26) yields

$$\begin{aligned}\vec{W}\cdot[(\vec{W}\cdot\nabla)(\vec{G} + \nabla\phi + \vec{U})] - (\vec{G} + \nabla\phi + \vec{U})\cdot\nabla\left(\frac{C^2}{2}\right) \\ -a^2\ [\nabla\cdot(\vec{G} + \nabla\phi + \vec{U})] \\ = -a^2\left(\frac{\gamma-1}{\gamma R}\right)(\vec{W}\cdot\nabla S) + \frac{1}{\rho}\ (\vec{W}\cdot\vec{\Sigma})\end{aligned} \tag{28}$$

Rearranging Equation (28), leaving only $\nabla\phi$ terms on the left-hand side, yields

$$\begin{aligned}\vec{W}\cdot[(\vec{W}\cdot\nabla)\nabla\phi] - \nabla\phi\cdot\nabla\left(\frac{C^2}{2}\right) - a^2\nabla\cdot(\nabla\phi) \\ = -\vec{W}\cdot[(\vec{W}\cdot\nabla)(\vec{G} + \vec{U})] + (\vec{G} + \vec{U})\cdot\nabla\left(\frac{C^2}{2}\right) \\ + a^2[\nabla\cdot(\vec{G} + \vec{U})] - a^2\left(\frac{\gamma-1}{\gamma R}\right)(\vec{W}\cdot\nabla S) \\ + \frac{1}{\rho}(\vec{W}\cdot\vec{\Sigma})\end{aligned} \tag{29}$$

However,

$$\nabla\cdot(\nabla\phi) = \nabla^2\phi \tag{30}$$

and therefore, Equation (29) finally becomes

$$\vec{W}\cdot[(\vec{W}\cdot\nabla)\nabla\phi] - a^2(\nabla^2\phi) - \nabla\phi\cdot\nabla\left(\frac{c^2}{2}\right)$$

$$= (\vec{G} + \vec{U})\cdot\nabla\left(\frac{c^2}{2}\right) - \vec{W}\cdot[(\vec{W}\cdot\nabla)(\vec{G} + \vec{U})]$$

$$+ a^2\nabla\cdot(\vec{G} + \vec{U}) - a^2\left(\frac{\gamma-1}{\gamma R}\right)(\vec{W}\cdot\nabla S) + \frac{1}{\rho}(\vec{W}\cdot\vec{\Sigma}) \qquad (31)$$

where all terms on the right-hand side of the equation are presumed known from previous computations.

Since viscous calculations are not the object of the current program, the appropriate equation for $\vec{U}$ will not be developed. However, this development parallels that given by Dodge[6]. A general outline of the required numerical method is given as follows:

- Establish grid system
- Calculate initial guess
- Calculate relaxation solution

These major sections of the present numerical method are described below.

Grid System

The choice of a grid system establishes many of the requirements for the subsequent calculations, as well as dictating the information and logic structure of the computer code. The inlet circulation gradient considerations, discussed in the preceding section, have an impact on this choice. Consider the grid system utilized by Dodge[6]. It is nonorthogonal on a succession of planes. Each plane, however, is orthogonal to a vector field formed from a set of quasi-streamlines. When large circulation gradients are present, such a grid system is not possible. To demonstrate this, consider the general equation for a surface in space.

$$f(x,y,z) = C_1 \qquad (32)$$

where C_1 is a constant.

A vector given by Equation (33)

$$d\vec{r} = dx\,\hat{x} + dy\,\hat{y} + dz\,\hat{z} \tag{33}$$

lies on a surface when

$$\frac{\partial f}{\partial x}\,dx + \frac{\partial f}{\partial y}\,dy + \frac{\partial f}{\partial z}\,dz = 0.$$

Without loss of generality it can be assumed that one coordinate direction has a non-zero derivative so that

$$dz = -\left(\frac{\partial f}{\partial x}\,dx + \frac{\partial f}{\partial y}\,dy\right) / \frac{\partial f}{\partial z} \tag{34}$$

or

$$d\vec{r} = dx\,\hat{x} + dy\,\hat{y} - \left(\frac{\partial f}{\partial x}\,dx + \frac{\partial f}{\partial y}\,dy\right) / \frac{\partial f}{\partial z}\,\hat{z} \tag{35}$$

If the surface, f, is to be normal everywhere to an arbitrary vector field, $\vec{V}$, then

$$d\vec{r}\cdot\vec{V} \equiv 0 \text{ for all directions given by dx and dy} \tag{36}$$

thus,

$$dx\,V_x + dy\,V_y - \left(\frac{\partial f}{\partial x}\,dx + \frac{\partial f}{\partial y}\,dy\right) V_z / \frac{\partial f}{\partial z} = 0. \tag{37}$$

or

$$dx\left(V_x\,\frac{\partial f}{\partial z} - V_z\,\frac{\partial f}{\partial x}\right) + dy\left(V_y\,\frac{\partial f}{\partial z} - \frac{\partial f}{\partial y}\,V_z\right) = 0. \tag{38}$$

Since dx and dy are arbitrary

$$\frac{V_x}{V_z} = \frac{\partial f/\partial x}{\partial f/\partial z} \tag{39a}$$

and

$$\frac{V_y}{V_z} = \frac{\partial f/\partial y}{\partial f/\partial z} \tag{39b}$$

it can be shown that Equations (39a) and (39b) hold only if Equation (40) holds.

$$\vec{V} \propto \nabla f \tag{40}$$

Therefore, there is not a single surface everywhere normal to a vector field unless that field is irrotational. Likewise, no simple single flow area exists describing any flow device, such as a low-hub-tip-ratio axial compressor. The view most utilized by compressor designers is the blade-to-blade section. Normals constructed across the channel cannot be stacked up into anything approaching a surface orthogonal to the streamwise direction. For the modern low-hub-tip-ratio compressor, this is anything but a small effect. Large differences in surface shapes occur between those constructed by dropping normals from the mean radius section, and those obtained by stacking blade-to-blade normals. Thus, one is forced to consider a grid system and a solution technique that is completely nonorthogonal. The grid system is selected by starting from the mean section (hub-to-shroud) on a user-selected master surface, which is also utilized for radial equilibrium calculations. This surface, running from hub to shroud, inlet to exit, but at a mean location between blades, is constructed to be two-dimensionally orthogonal (X2-X3 plane, where X1 is blade-to-blade, X2 hub-to-shroud, and X3 inlet-to-exit directions). The grid system is then constructed from normals in the blade-to-blade direction. This conforms with the normal two-dimensional practice in turbomachinery. Blade-to-blade projections will have the appearance (but not the reality) of being orthogonal. Hub-to-shroud views will clearly be nonorthogonal in cases where appreciable spanwise circulation gradients exist. Such an example is shown in Figure 6 for an axial inlet similar to that of Figure 4.

Once the basic pattern of the grid system has been selected, the actual mechanics of the generation must be developed. Dodge[6] basically used a two-step process.

(1) Generate quasi-streamlines.

(2) Carve the streamlines by projecting normals from known points to unknown points.

Both processes consume considerable amounts of computer time in the program developed by Dodge[6]. Some effort was expended to speed up this process, resulting in approximately a 30 to 1 improvement. A brief discussion of this new method follows.

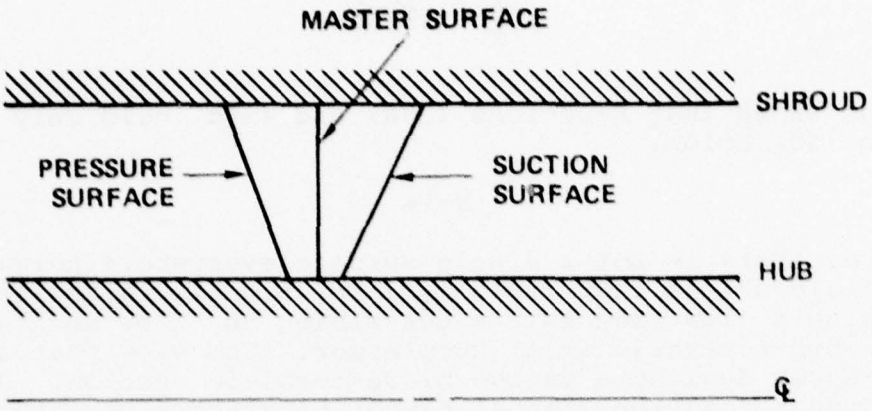

SIDE VIEW OF GRID LINES ON THE EXTREME BLADE SURFACES AND MASTER SURFACE

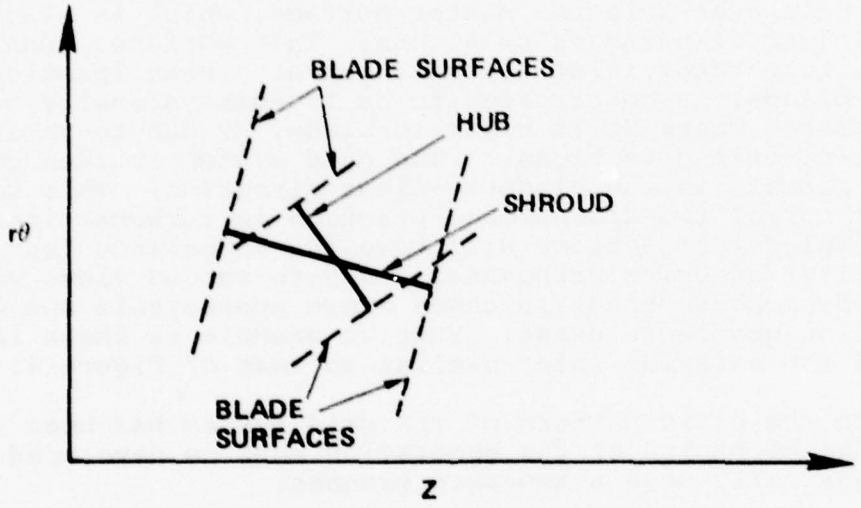

Figure 6. Projections of Grid Lines For An Axial Inlet-Rotating Frame

A computer code can be viewed as an information processor. The code starts with what is usually a very limited amount of information contained in the input deck. It is then expanded, utilized, and ultimately compacted back to an amount small enough for the human mind to quickly assimilate the results. Input geometry typifies this process. The user describes only the boundary surfaces. The computer fills out the rest of the grid system by laying in a bundle of quasi-streamlines. However this is accomplished, the quasi-streamlines can only be a function of the input data points. Equation (41) must represent a general relation between a point on a quasi-streamline and the input data.

$$X_i = \sum_{j=1}^{N} f_{ji} x_j \qquad (41)$$

where

X_i = coordinate on a quasi-streamline
x_j = input blade surface coordinate
f_{ji} = influence coefficient

The method used by Dodge[6] to obtain quasi-streamlines involved solving a number of 2-D stream-function problems to first determine surfaces of revolution and then to establish blade-to-blade streamlines. The current program uses an interpolative method. Surfaces of revolution are determined by interpolation between hub and shroud on an equal area basis. Likewise, blade-to-blade surfaces are established by blade-to-blade interpolation. It would be expected that these interpolation factors could not be independent for every such surface. Thus, an efficient approach is to obtain a final set of influence coefficients (Equation 41) by a convolution of hub-to-shroud and blade-to-blade factors. Then the actual streamline points can be calculated by the long vector multiplication and addition of Equation (41). Such an approach eliminates much of the overhead that creeps into other more fragmented approaches.

Once quasi-streamlines have been obtained, they must be cut into a grid system by casting normals from selected streamlines to neighbors. The algorithm to accomplish this utilizes the following steps:

- Establish the order of connection of quasi-streamlines. The grid point on any quasi-streamline is placed by constructing a normal from a neighboring quasi-streamline with known points. The order of this connection in a single X3-plane is shown in Figure 7.

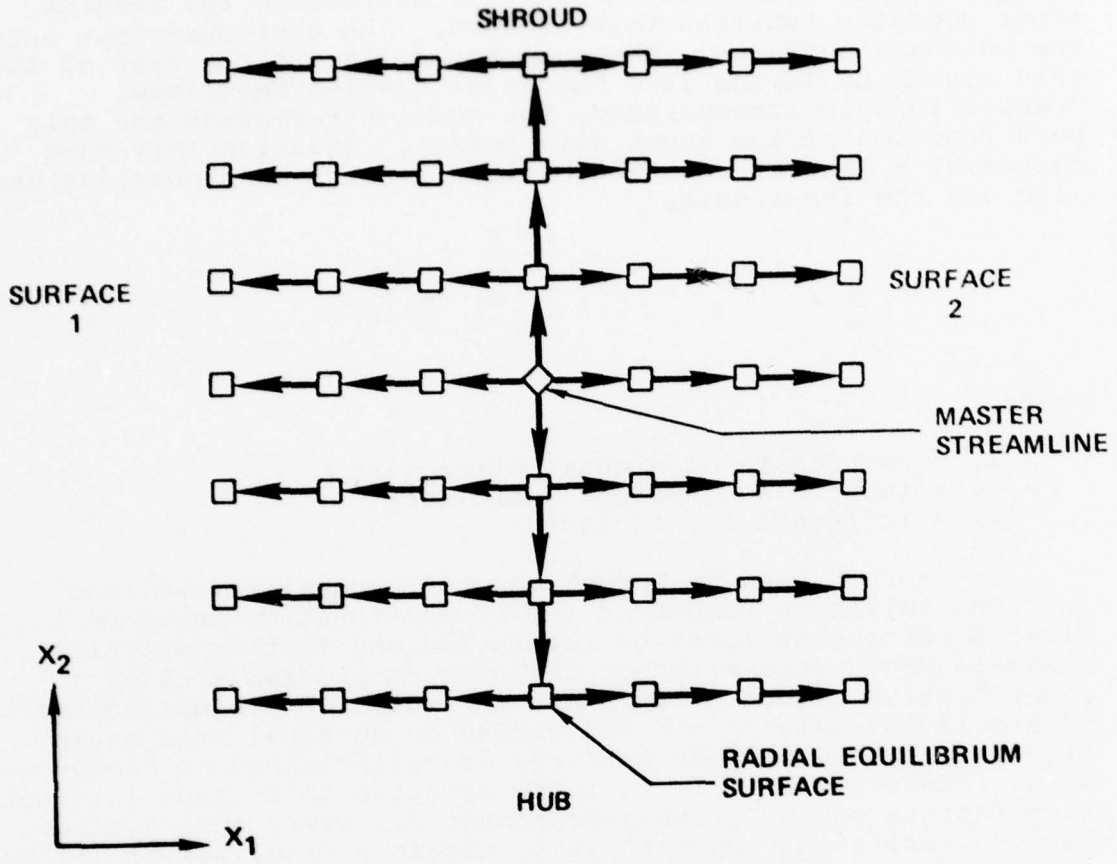

Figure 7. The Order of Connection of Grid Points on a X3 Surface

- Reorder the quasi-streamline definition to line up with established grid connection.

- Compute the fractional location, S_i, of normals from quasi-streamline points to their connected neighbors and assure that this array is ordered (see Figure 8).

- Compute actual grid points by establishing the spacing on the master streamline. Then interpolate in the table of normals to find the location of the next point.

Such an algorithm minimizes calculations by calculating normals on grid lines that actually connect; calculating normals based on the input quasi-streamline points, which are usually much less in number than grid points; and by arranging data structure to allow vectorized loops.

Initial-Guess Solution

The natural initial-guess solution is based on a 2-D solution on a hub-to-shroud surface. Such solution techniques were developed in the early 50's by Wu[7]. Since that time, they have been highly refined using both finite-difference and curvature-of-streamline techniques. However, if the mean surface shape is specified, the governing stream function undergoes an obvious elliptic-to-hyperbolic transition as the Mach number passes through unity (in the relative frame). Because of this, solution techniques have concentrated on the specified work formulation, which remains elliptic until the meridional component of velocity becomes supersonic. However, the work form is inconvenient when analyzing an already existing geometry, since it is difficult to relate a particular shape to a work distribution. For these reasons, a transonic relaxation solution to a Wu-type stream-function equation was developed. An outline of the technique follows.

The basic equation to develop a stream-function solution is the rotating version of the Crocco-Vazsonyi equation as given by Owczarek[8].

$$2(\vec{\omega}\times\vec{W}) - \vec{W}\times(\nabla\times\vec{W}) = -\nabla I + T\nabla S + \vec{\Sigma}/\rho \qquad (42)$$

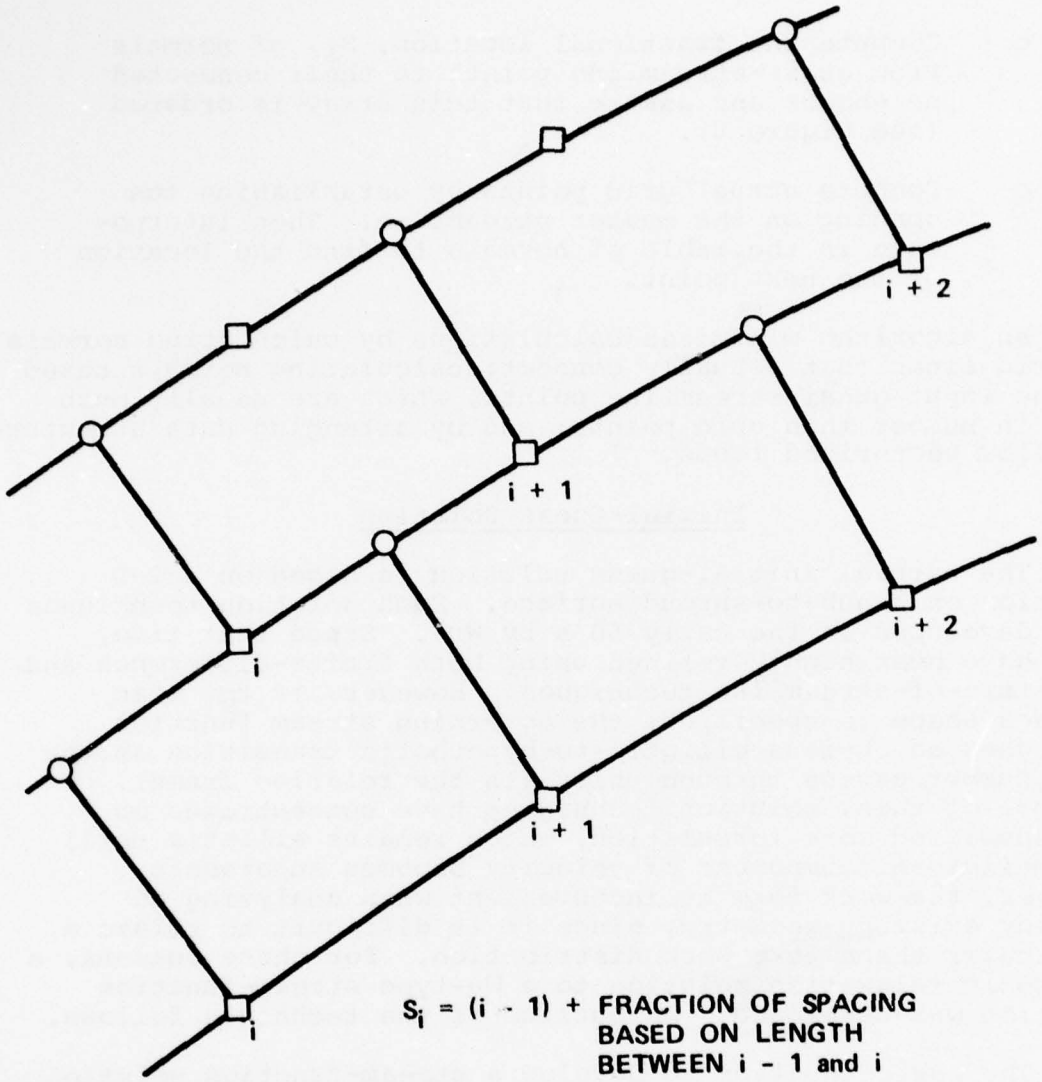

Figure 8. Normal Location on the Neighbors

where

$\vec{W}$ = velocity vector

$\vec{\omega}$ = rotational vector

I = rothalpy

T = static temperature

S = entropy

$\vec{\Sigma}$ = viscous stress vector

ρ = density

Wu concentrated on cylindrical coordinates. To be useful for all configurations, an equivalent form in arbitrary curvilinear coordinates is required. Only one component of Equation (43) is actually utilized; in this case, the component in the X_2 direction. It is assumed that flow only exists parallel to the master surface, yielding $W_1 \equiv 0$.

8

$$- W_3 \left[\frac{1}{h_2} \frac{\partial W_3}{\partial X_2} - \frac{1}{h_3} \frac{\partial W_2}{\partial X_3} + \frac{W_3}{h_2 h_3} \frac{\partial h_3}{\partial X_2} - \frac{W_2}{h_2 h_3} \frac{\partial h_2}{\partial X_3} \right] - 2\omega_1 W_3$$

$$= \frac{T}{h_2} \frac{\partial S}{\partial X_2} - \frac{1}{h_2} \frac{\partial I}{\partial X_2} + \frac{\Sigma_2}{\rho} \tag{43}$$

A stream function can be defined that automatically solves continuity.

$$\frac{1}{h_2} \frac{\partial \Psi}{\partial X_2} = \rho B W_3 \tag{44}$$

$$\frac{1}{h_3} \frac{\partial \Psi}{\partial X_3} = -\rho B W_2 \tag{45}$$

where B is a factor to take into account blade-to-blade streamsheet convergence.

From these equations, one can follow Wu's development directly, yielding a stream-function equation given by Equation (46)

$$(a^2-W_2^2)\ \frac{1}{h_2^2}\ \frac{\partial^2\Psi}{\partial X_2^2} - \frac{2W_2W_3}{h_2h_3}\ \frac{\partial^2\Psi}{\partial X_2\partial X_3} + (a^2-W_3^2)\ \frac{1}{h_3^2}\ \frac{\partial^2\Psi}{\partial X_3^2}$$

$$+ \frac{N}{h_2}\ \frac{\partial\Psi}{\partial X_2} + \frac{M}{h_3}\ \frac{\partial\Psi}{\partial X_3} = 0. \qquad (46)$$

where

$$N = (a^2-W^2)\ \left\{\frac{1}{W_3^2}\ \left[\frac{T_2}{h_2}\ \frac{\partial S}{\partial X_2} - \frac{1}{h_2}\ \frac{\partial I}{\partial X_2} + \frac{\Sigma_2}{\rho}\right.\right.$$

$$\left.\left. + 2W_3\omega_1 - \frac{W_3^2}{h_2h_3}\ \frac{\partial h_3}{\partial X_2}\right] - \frac{1}{h_2^2}\ \frac{\partial h_2}{\partial X_2}\right\} - \frac{W_3^2}{h_2^2}\ \frac{\partial h_2}{\partial X_2} - \frac{W_2^2}{h_2h_3}\ \frac{\partial h_3}{\partial X_2}$$

$$- \frac{1}{h_2}\ \frac{\partial}{\partial X_2}\ \left(I + \frac{C^2}{2}\right)\ -\ \frac{a^2}{h_2}\ \left[\frac{\partial \ln B}{\partial X_2} - \frac{\partial(S/R)}{\partial X_2}\right]$$

$$M = (a^2-W^2)\ \left\{\frac{1}{h_2h_3}\ \frac{\partial h_2}{\partial X_3} - \frac{1}{h_3^2}\ \frac{\partial h_2}{\partial X_3}\right\}$$

$$- \frac{1}{h_3}\ \frac{\partial}{\partial X_3}\ \left(I+\frac{C^2}{2}\right) - \frac{a^2}{h_3}\ \left[\frac{\partial \ln B}{\partial X_3} - \frac{\partial(S/R)}{\partial X_3}\right]$$

$$- \frac{W_3^2}{h_2h_3}\ \frac{\partial h_2}{\partial X_3} - \frac{W_2^2}{h_3^2}\ \frac{\partial h_3}{\partial X_3}$$

$$C = \omega r$$

$$I = h + \frac{W^2}{2} - \frac{C^2}{2} = h_o' - C_oV_{\theta o}$$

h_o' = stagnation enthalpy at the streamline inlet

$V_{\theta o}$ = absolute preswirl

The solution procedure is essentially similar to that for potential equations. The coefficients are computed from Equation (46). The result is then a coefficient matrix whose region of influence is controlled by the local Mach number with boundary conditions which specify Ψ on all boundaries. The stream function is then differentiated to form a ρW product which can be two-valued in W. Both supersonic and subsonic solutions are obtained by nondimensionalizing the ρW curves to the form given by Equation (47).

$$G = \frac{\rho W}{\rho'' a''} = \frac{W^*}{\sqrt{\gamma-1}} \left(1 - \frac{W^{*2}}{2}\right)^{1/\gamma-1} \tag{47}$$

where

$W^* = W/\sqrt{h''}$

ρ'' = stagnation density in the relative frame

h'' = stagnation enthalpy in the relative frame

$a'' = \sqrt{(\gamma-1)h''}$

Both the subsonic and supersonic velocities are obtained from approximation to an inverse of Equation (47), as given by Equation (48) for subsonic flow and (49) for supersonic flow.

$$W_1^* = W_m^* \left[1 - (1-G/G_m)^{\beta_1}\right] \tag{48}$$

$$W_2^* = \left[\sqrt{2}-W_m^*\right]\left[1-G/G_m\right]^{\beta_2} + W_m^* \tag{49}$$

where

$$G_m = \left(\frac{2}{\gamma+1}\right)^{\frac{\gamma+1}{2(\gamma-1)}}$$

$$W_m = \sqrt{\frac{2(\gamma-1)}{\gamma+1}}$$

G_m and W_m represent the maximum value of flow and the velocity at this maximum, respectively.

One must still decide which solution to select. This is accomplished based on a direct analogy to potential solution. A potential-like parameter is computed along streamlines from inlet to exit by computing the following:

$$\Gamma(\Psi) = \int_{\text{Inlet}}^{\text{Exit}} W\, h_3 dx_3 \tag{50}$$

The following conditions can be applied to W, depending on the case.

Case	$\Gamma(\Psi)$
Subsonic Throughout	Irrelevant--always take W_1^*
Supersonic In Subsonic out	Read a desired value of $\Gamma(\Psi)$, make a transition from W_2^* to W_1^* at the point yielding an exit integral of $\Gamma(\Psi)$ equal to that desired.
Supersonic Tip Subsonic Hub	On hub use subsonic value throughout. An exit-circulation spanwise Γ variation is then specified
Subsonic In Supersonic Out	Make transition at minimum area location
Supersonic In Supersonic Out	Use only supersonic values

With the specification of these conditions, a solution to the flow on the mean stream surface is provided. For cases with supersonic in and subsonic out, the actual shock location is arbitrarily dependent on the choice of the circulation parameter. In these cases, the initial guess may be too realistic. To illustrate, consider the equivalent of Equation (31) for flow in a 1-D duct with area variations.

$$(W^2-a^2)\ \frac{d^2\phi}{dx^2} - a^2\ \frac{d\phi}{dx}\ \frac{1}{A'}\ \frac{dA'}{dx} = a^2 G\ \frac{1}{A'}\ \frac{dA'}{dx} - (W^2-a^2)\ \frac{dG}{dx} \qquad (51)$$

where

$$\frac{1}{A'}\ \frac{dA'}{dx} = \frac{1}{A}\ \frac{dA}{dx} - \left(\frac{\gamma-1}{\gamma R}\right)\ \frac{dS}{dx}$$

A is the cross-sectional area

For this case, entropy changes are indistinguishable from area variations. Considering the diverging portion of a converging-diverging nozzle at a high back pressure, a shock stands in the nozzle. Flow upstream and downstream of this shock approximately obeys the 1-D equations. Across the shock the Rankine-Hugoniot relations apply. The actual location of the shock is fixed by establishing the precise points where the Rankine-Hugoniot relation is in balance with upstream and downstream solutions. If the guess is very good, such as solving isentropic relations both ahead of and behind a discontinuity arbitrarily located, then any adjustment in shock position must be accomplished by recognizing the error at the shock. This error must then propagate to the whole flow field, as indicated schematically in Figure 9. There are several problems in obtaining such a solution. The first of these is requiring an isentropic rise, as well as fall, in the potential solution. The star-switching methods in use discriminate against such potential rises. Additionally, the error is only at the guessed discontinuity and it must propagate out to the rest of the field. Figure 10 shows the results that actually occur for such a guess (1st calculation). Except in the region of the discontinuity, little potential correction occurs. A much better choice is to connect input to output by a straight line yielding continuous flows and relatively large differences between guessed and final solutions everywhere. This approach is used for the full three-dimensional solutions described in Section III.

The mean surface solution is projected to the surfaces by utilizing Equation (52).

$$G_3\ (X_1,\ X_2) = G_{3m}\ (X_2)\ h_{3m}/h_3 \qquad (52)$$

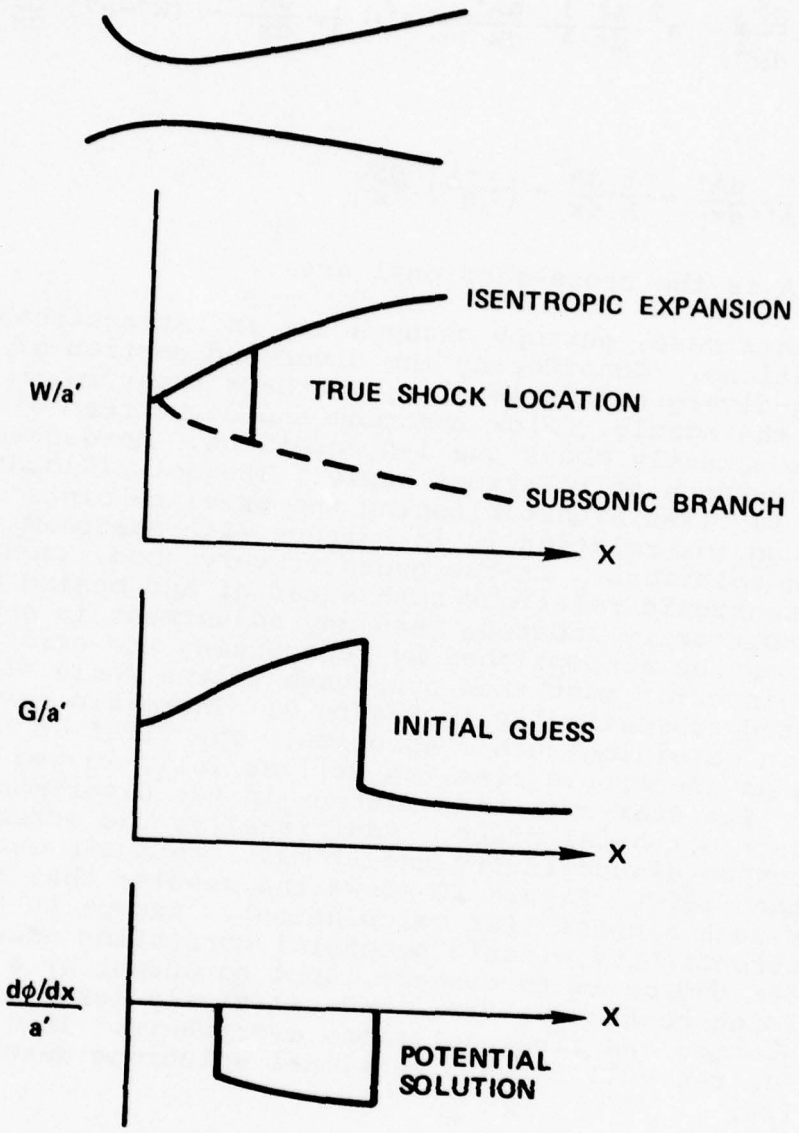

Figure 9. The Effect of a Good Initial Guess

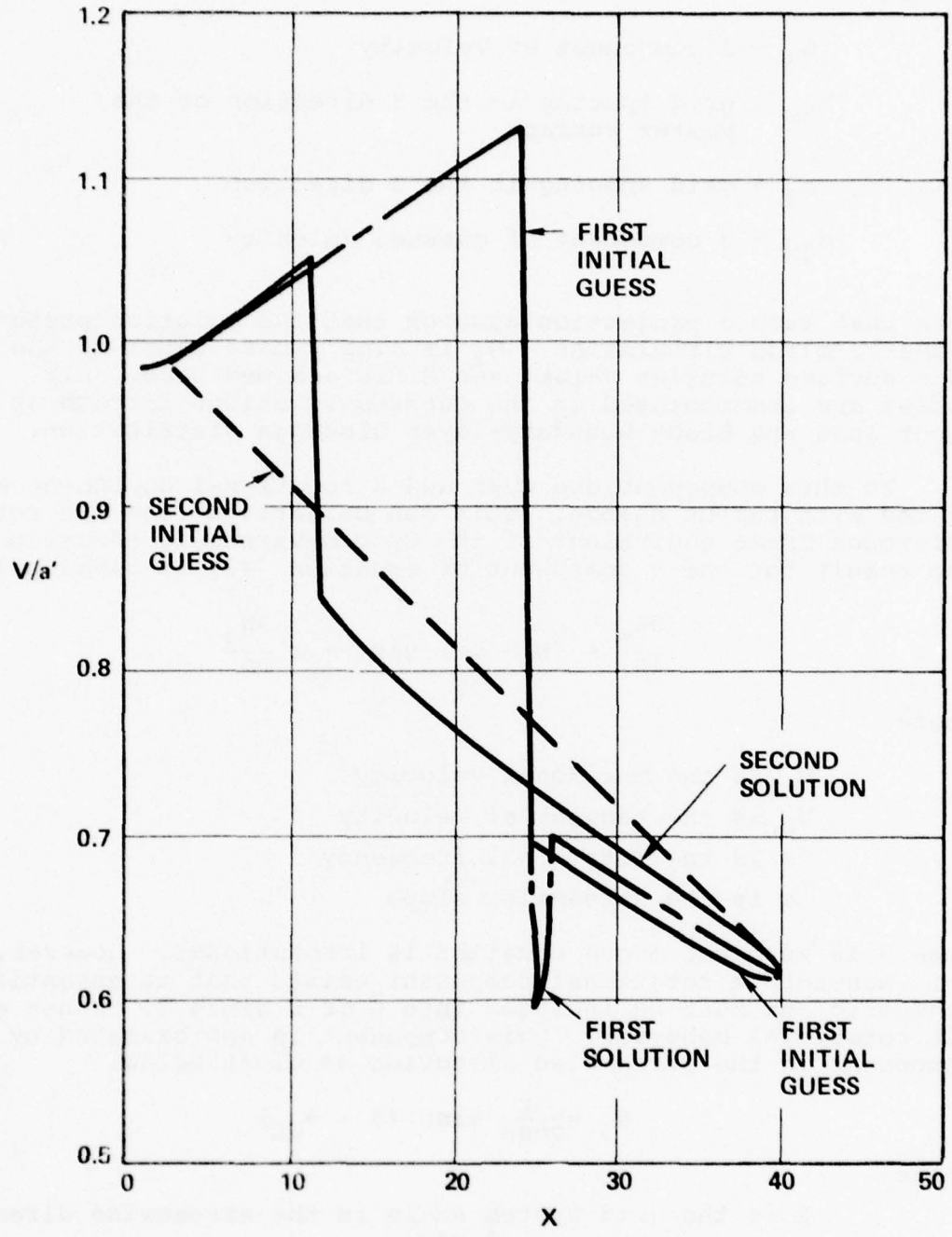

Figure 10. Solutions for Near Isentropic Cases

where

G_3 = 3 component of velocity

h_{3m} = grid spacing in the 3 direction on the master surface

h_3 = grid spacing in the 3 direction

G_{3m} = 3 component of guessed velocity

Note that such a projection assures that the solution preserves blade-to-blade circulation. G_2 is simply made equal to the mean surface solution value, and G_1 is assumed zero. All losses are incorporated in the guessed solutions through an input loss and blade boundary-layer blockage distribution.

To this component one must add a rotational component associated with radius change. This can be derived from the rotating reference frame equivalent of the Crocco-Vazsonyi, equation (42). The result for the θ component of equation (42) is given below.

$$\frac{\partial W_m}{\partial \theta} = (W_\theta + \omega r) \sin\alpha + r \frac{\partial W_\theta}{\partial m}$$

where

W_m is the meridonal velocity

W_θ is the tangential velocity

ω is the rotational frequency

α is the streamline slope

When ω is zero the above equation is irrotational. However, when ω is non-zero a rotational component exists that is essentially geometric and must be included into $\vec{G}$ or $\vec{U}$ since $\nabla\phi$ cannot exhibit rotational behavior. This component is approximated by a U component in the streamwise direction as given below.

$$U_3 = \frac{\omega r}{\cos\beta} \sin\alpha \, (\theta - \theta_{CL})$$

where

β is the grid system angle in the streamwise direction given by $\beta = \tan^{-1}(\frac{rd\theta}{dm})$

θ_{CL} is the value of θ on the master surface across the blade passage

This component is wholly geometric, zero on the master surface, and is simply added to the results of Equation (52).

Potential Solution

The potential solution proceeds in a similar fashion to that described by Dodge[6]. However, the use of a completely non-orthogonal grid seriously complicates the geometry considerations.

Equation (31) represents a general vector form of the partial differential equation for potential, which may now be expressed in Cartesian coordinates as follows.

$$(W_x^2 - a^2)\frac{\partial^2\phi}{\partial x^2} + W_x W_y \frac{\partial^2\phi}{\partial x\partial y} + W_x W_z \frac{\partial^2\phi}{\partial x\partial z} + W_y W_x \frac{\partial^2\phi}{\partial y\partial x}$$

$$+ (W_y^2 - a^2)\frac{\partial^2\phi}{\partial y^2} + W_y W_z \frac{\partial^2\phi}{\partial y\partial z} + W_z W_x \frac{\partial^2\phi}{\partial z\partial x} + W_z W_y \frac{\partial^2\phi}{\partial z\partial y}$$

$$+ (W_z^2 - a^2)\frac{\partial^2\phi}{\partial z^2} - \omega^2 x \frac{\partial\phi}{\partial x} - \omega^2 y \frac{\partial\phi}{\partial y} = \omega^2 x (G_x + U_x)$$

$$+ \omega^2 y (G_y + U_y) - (W_x^2 - a^2)\frac{\partial}{\partial x}(G_x + U_x) - W_x W_y \frac{\partial}{\partial y}(G_x + U_x)$$

$$- W_x W_z \frac{\partial}{\partial z}(G_x + U_x) - W_y W_x \frac{\partial}{\partial x}(G_y + U_y)$$

$$- (W_y^2 - a^2)\frac{\partial}{\partial y}(G_y + U_y) - W_y W_z \frac{\partial}{\partial z}(G_y + U_y)$$

$$- W_z W_x \frac{\partial}{\partial x}(G_z + U_z) - W_z W_y \frac{\partial}{\partial y}(G_z + U_z)$$

$$- (W_z^2 - a^2)\frac{\partial}{\partial z}(G_z + U_z) - a^2\left(\frac{\gamma-1}{\gamma R}\right)\left[W_x \frac{\partial S}{\partial x} + W_y \frac{\partial S}{\partial y}\right.$$

$$\left. + W_z \frac{\partial S}{\partial z}\right] + \frac{1}{\rho}(W_x \Sigma_x + W_y \Sigma_y + W_z \Sigma_z) \qquad (53)$$

Equation (53) represents the partial differential equation for perturbation potential in Cartesian coordinates. The equation is elliptic for subsonic conditions and hyperbolic for supersonic conditions. Thus, it is adaptable to solution by relaxation techniques.

Boundary Conditions on Perturbation Potential - At the inlet and outlet of the blade passage, the perturbation potential, ϕ, is assumed to be equal to zero. This is a valid assumption when the inlet and outlet are chosen far enough from the blades that the radial equilibrium solution provides a satisfactory representation of the flow. On solid surfaces, and bounding streamlines, the boundary condition on ϕ is

$$\nabla\phi \cdot \vec{n} = 0 \tag{54}$$

or, expanding in Cartesian coordinates

$$n_x \frac{\partial\phi}{\partial x} + n_y \frac{\partial\phi}{\partial y} + n_z \frac{\partial\phi}{\partial z} = 0 \tag{55}$$

Cartesian-to-Nonorthogonal Coordinate Transformation - Equation (53) is expressed in terms of Cartesian coordinates; however, the grid system generated within the program is nonorthogonal. Thus, in order to formulate difference schemes in the nonorthogonal grid, the Cartesian derivatives in Equation (53) must be recast in terms of derivatives with respect to nonorthogonal coordinates. A transformation matrix to accomplish this was developed as follows.

Consider a scalar property A. The differential of A with respect to Cartesian coordinates is:

$$dA = \frac{\partial A}{\partial x} dx + \frac{\partial A}{\partial y} dy + \frac{\partial A}{\partial z} dz = \sum_{j=1}^{3} \frac{\partial A}{\partial X_j} dX_j \tag{56}$$

where

$$(X_1, X_2, X_3) = (x, y, z)$$

Equation (56) provides the basis for expressing derivatives in the nonorthogonal coordinate directions (x_1, x_2, x_3). The partial derivative of A, with respect to the nonorthogonal direction x_i, may then be formed from Equation (56):

$$\frac{\partial A}{\partial x_i} = \sum_{j=1}^{3} \frac{\partial A}{\partial X_j} \frac{\partial X_j}{\partial x_i} \text{ for } i = 1, 2, 3 \tag{57}$$

Second derivatives may be treated similarly, with the differential written in Cartesian coordinates as:

$$d\left(\frac{\partial A}{\partial x_i}\right) = \sum_{k=1}^{3} \frac{\partial}{\partial X_k}\left(\frac{\partial A}{\partial x_i}\right) dX_k \quad \text{for } i = 1, 2, 3 \tag{58}$$

Then, the partial derivative of $\frac{\partial A}{\partial x_i}$, with respect to the non-orthogonal direction x_ℓ, becomes

$$\frac{\partial}{\partial x_\ell}\left(\frac{\partial A}{\partial x_i}\right) = \sum_{k=1}^{3} \frac{\partial}{\partial X_k}\left(\frac{\partial A}{\partial x_i}\right) \frac{\partial X_k}{\partial x_\ell} \quad \begin{matrix} \text{for } i = 1, 2, 3 \\ \ell = 1, 2, 3 \end{matrix} \tag{59}$$

Substituting Equation (57) into Equation (59) yields the following:

$$\frac{\partial}{\partial x_\ell}\left(\frac{\partial A}{\partial x_i}\right) = \sum_{k=1}^{3} \frac{\partial}{\partial X_k}\left[\sum_{j=1}^{3} \frac{\partial}{\partial X_j}\frac{\partial X_j}{\partial x_i}\right] \frac{\partial X_k}{\partial x_\ell} \tag{60}$$

or, expanding Equation (60)

$$\frac{\partial}{\partial x_\ell}\left(\frac{\partial A}{\partial x_i}\right) = \sum_{k=1}^{3}\sum_{j=1}^{3} \left(\frac{\partial^2 A}{\partial X_k \partial X_j}\right) \frac{\partial X_j}{\partial x_i}\frac{\partial X_k}{\partial x_\ell}$$

$$+ \sum_{k=1}^{3}\sum_{j=1}^{3} \left(\frac{\partial A}{\partial X_j}\right) \frac{\partial}{\partial X_k}\left(\frac{\partial X_j}{\partial x_i}\right) \frac{\partial X_k}{\partial x_\ell}$$

$$\begin{matrix} \text{for } i = 1, 2, 3 \\ \ell = 1, 2, 3 \end{matrix} \tag{61}$$

In Equation (61), the geometry derivative $\frac{\partial}{\partial X_k} \frac{\partial X_j}{\partial x_i}$ must be recast in terms of nonorthogonal derivatives. This conversion is performed by rewriting the second term of Equation (61) as:

$$\sum_{k=1}^{3} \sum_{j=1}^{3} \left(\frac{\partial A}{\partial X_j}\right) \frac{\partial}{\partial X_k} \left(\frac{\partial X_j}{\partial x_i}\right) \frac{\partial X_k}{\partial x_\ell} = \sum_{j=1}^{3} \left(\frac{\partial A}{\partial X_j}\right) \left[\sum_{k=1}^{3} \frac{\partial}{\partial X_k} \left(\frac{\partial X_j}{\partial x_i}\right) \frac{\partial X_k}{\partial x_\ell} \right]$$

and then employing Equation (57) to replace the term in brackets:

$$\sum_{k=1}^{3} \frac{\partial}{\partial X_k} \left(\frac{\partial X_j}{\partial x_i}\right) \frac{\partial X_k}{\partial x_\ell} = \frac{\partial}{\partial x_\ell} \left(\frac{\partial X_j}{\partial x_i}\right)$$

Then, the final form of Equation (61) is

$$\frac{\partial}{\partial x_\ell} \left(\frac{\partial A}{\partial x_i}\right) = \sum_{k=1}^{3} \sum_{j=1}^{3} \left(\frac{\partial^2 A}{\partial X_k \partial X_j}\right) \frac{\partial X_j}{\partial x_j} \frac{\partial X_k}{\partial x_\ell}$$

$$+ \sum_{j=1}^{3} \left(\frac{\partial A}{\partial X_j}\right) \left[\frac{\partial}{\partial x_\ell} \left(\frac{\partial X_j}{\partial x_i}\right)\right] \quad \text{for } i = 1, 2, 3 \quad \ell = 1, 2, 3 \qquad (62)$$

A 12 x 12 transformation matrix may be built to represent Equation (62):

$$T = \left[\begin{array}{c:c} \dfrac{\partial X_j}{\partial x_i}\dfrac{\partial X_k}{\partial x_\ell} & \dfrac{\partial}{\partial x_\ell}\left(\dfrac{\partial X_j}{\partial x_i}\right) \\ (9 \times 9) & (9 \times 3) \\ \hdashline --0-- & \dfrac{\partial X_j}{\partial x_i} \\ (3 \times 9) & (3 \times 3) \end{array}\right]$$

Defining the 12-element derivative vectors as

$$\vec{d} = \begin{bmatrix} \dfrac{\partial^2 A}{\partial x_\ell \partial x_i} \\ \cdots\cdots \\ \dfrac{\partial A}{\partial x_i} \end{bmatrix} \qquad \vec{D} = \begin{bmatrix} \dfrac{\partial^2 A}{\partial X_k \partial X_j} \\ \cdots\cdots \\ \dfrac{\partial A}{\partial X_j} \end{bmatrix}$$

Equation (62) is represented as

$$\vec{d} = T\vec{D} \tag{63}$$

Then, by taking the inverse of T, the derivatives with respect to Cartesian coordinates may be expressed in terms of derivatives with respect to nonorthogonal coordinates:

$$\vec{D} = T^{-1} \vec{d} \tag{64}$$

Equation (64) thus provides the necessary transformation expression for the conversion of derivatives in Equations (53) and (55) to nonorthogonal coordinates.

Numerical Method for Solution of Potential Equation - The partial differential equation governing perturbation potential [Equation (53)] is recast as a linear difference equation in nonorthogonal coordinates. The difference technique is described in Appendix A. The resulting linear system may then be solved by relaxation techniques.

The difference star used employs 40 nodes, and is capable of treating derivatives at all interior and boundary nodes. It produces a centered difference scheme in the streamwise direction for subsonic flow, and a mixed-hyperbolic and implicit scheme in the presence of supersonic flow. The degree of mixing is determined as a function of local Mach number, based upon a criterion developed from a stability analysis of the basic relaxation difference equation. As Mach number increases, the variable supersonic difference star becomes weighted to more closely reflect the region of influence of the characteristic lines, eventually becoming totally hyperbolic.

Program Architecture - In designing this program, a primary goal was to maintain the capability of handling problems to a maximum size of 10,000 nodes. In order to accomplish this on the CY174, it became necessary to introduce sequential files within the relaxation module to handle large data blocks, such as grid-transformation arrays and coefficient arrays. In addition, smaller data blocks were stored on random files managed by the scratch information processor. A general logic diagram of the potential equation solution module is given in Figure 11.

The relaxation iteration package utilized in this program consists of an optimized assembly language routine, which performs ordinary over-relaxation and permits the entire problem to be held within core memory during iteration. The assembly language routine is more than three times faster than the Fortran routine that it replaces.

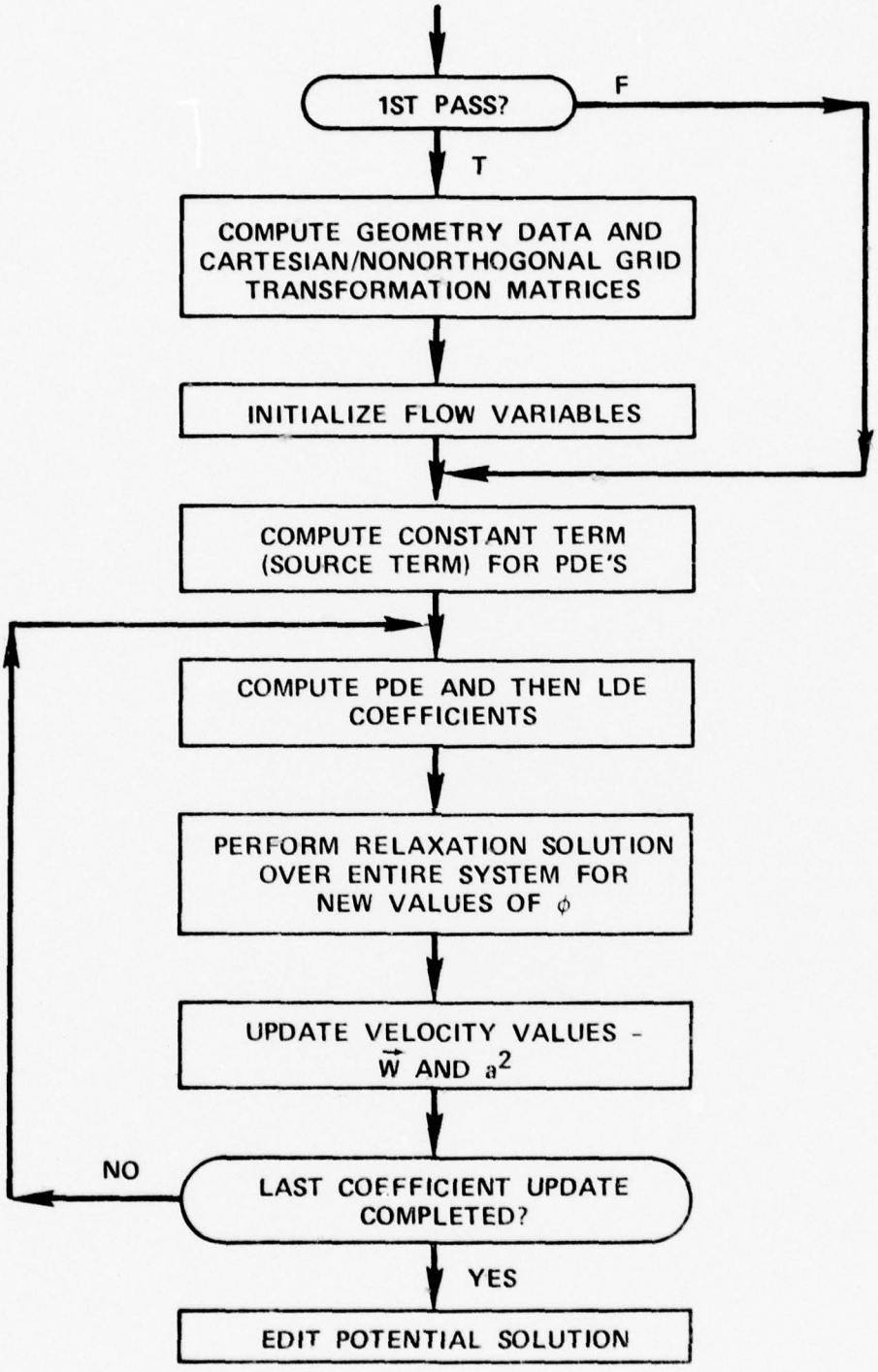

Figure 11. Logic Diagram for Potential Equation Solution Module

SECTION III

RESULTS

The USAF has had a program to develop high-pressure-ratio, high-diffusion axial compressors for several years. In particular, the program of interest involved a rotor designed for a 3.0 to 1.0 pressure ratio in a 1600 ft/sec axial stage. Initial tests of this device indicated that deviation angles were excessive without a second partial-flow splitter near the exit. A center-section from this rotor was tested with a splitter and the results were reported by Holtman et al[9]. Dodge[10] later studied this cascade utilizing two-dimensional transonic relaxation methods. The rotor was designed by Wennerstrom and Frost[11], and the test results were reported by Wennerstrom et al[12]. Although the computer program developed herein is expected to have much wider application than these devices, the motivation for its development rests in certain inabilities to design such high work stages.

Although the splitter had substantial benefits, its cascade test indicated that rather severe diffusions occur. However, questions existed as to the applicability of the cascade test. The extreme convergence of the stage required contracting relatively low-aspect-ratio end walls applied to a supersonic cascade. This configuration introduces a complex interaction between curvatures simultaneously occurring in two directions. The intent of this program was to explore these questions by analysis. The results of this study are described below, beginning with a conventional transonic cascade, then high-turning cascades, and finally a rotor.

VKI Low-Camber Cascade

In 1973, as part of a von Karman Institute short course, Breugelmans and Starken[13] reported data on a low-camber DCA airfoil. As a test case, a two-bladed cascade configuration was calculated at an inlet Mach number of 1.409. The grid system along the centerline is shown in Figure 12. Note that the two side walls are formed by the suction and pressure surface of the cascade. The resultant solution is shown in Figure 13. The center blade and outside wall show very similar pressure distributions. However, the pressure surface of the center blade indicates some of the previously unpredictable acceleration near the leading edge. Two data cases bracketing the calculated static pressure ratio are compared to the center blade loading in Figure 14.

The one very low static pressure point on the suction surface just ahead of the trailing edge is considered spurious, since it does not appear on any other sections. Agreement is as good as the comparisons between time-dependent and non-orthogonal relaxation methods, presented by Dodge[1] previously,

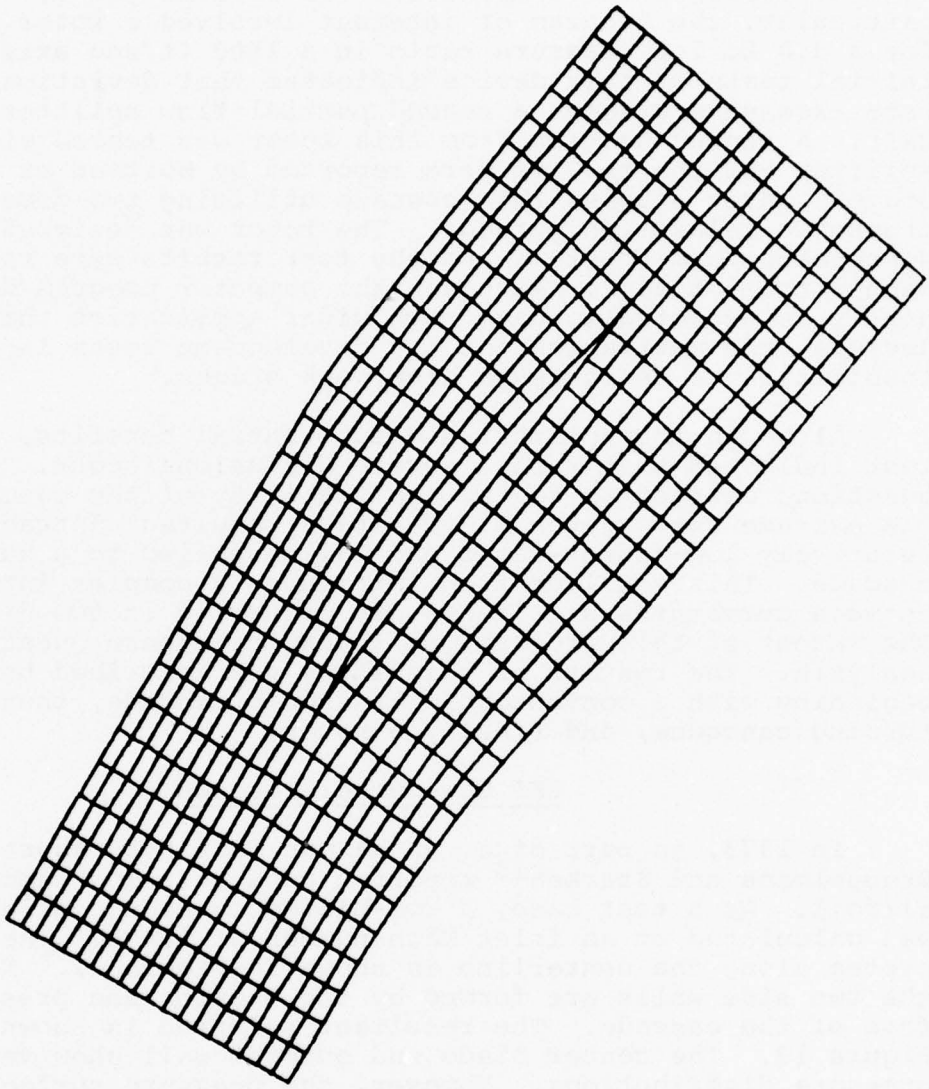

Figure 12. Centerline Grid System VKI Low-Camber DCA Cascade, M_I = 1.409, β_2 = 47.0 Degrees

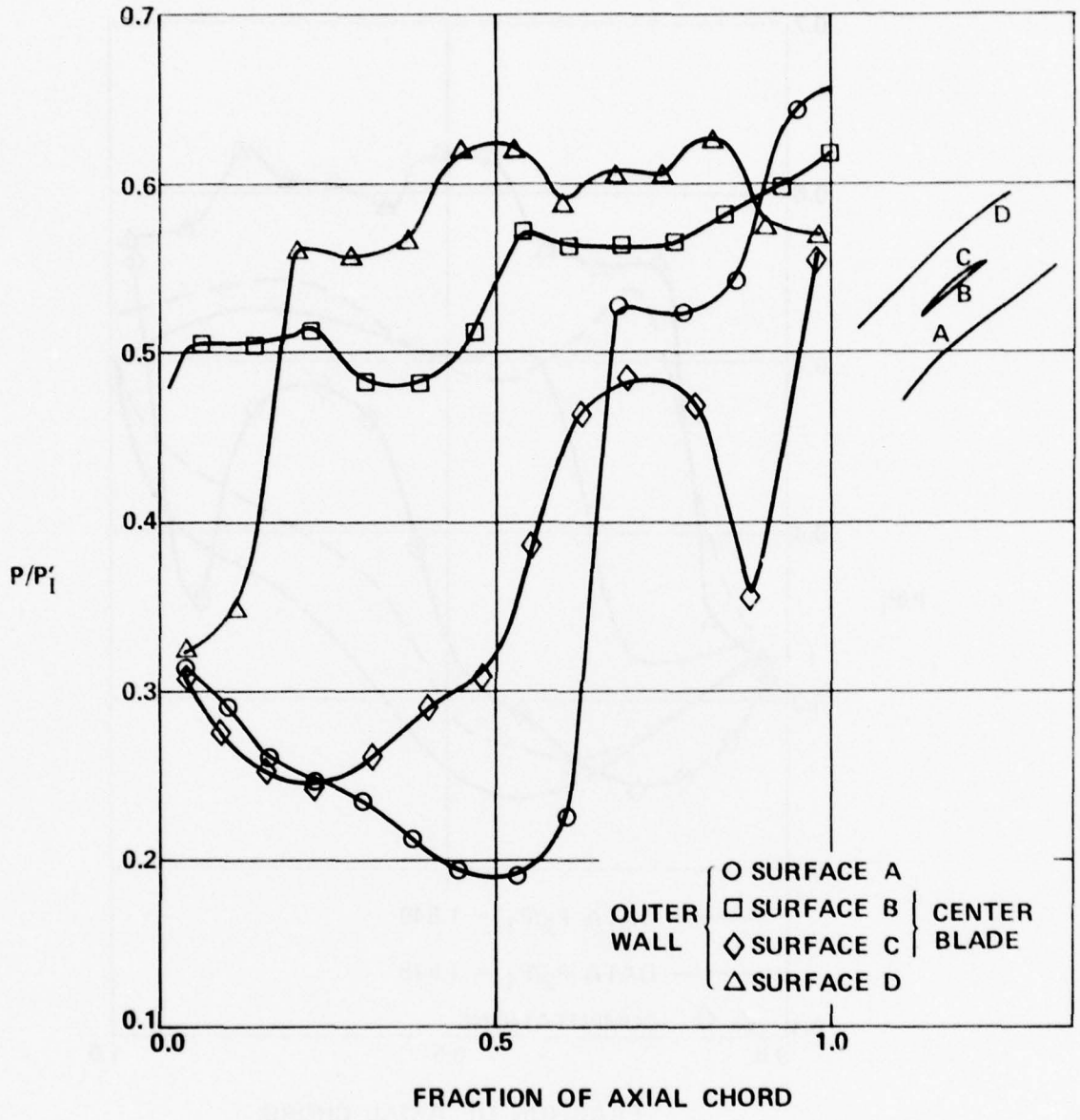

Figure 13. Static Pressure Ratios Calculated on Two-Blade VKI 9.5-Degree Camber Cascade, β_2 = 49.0 Degrees

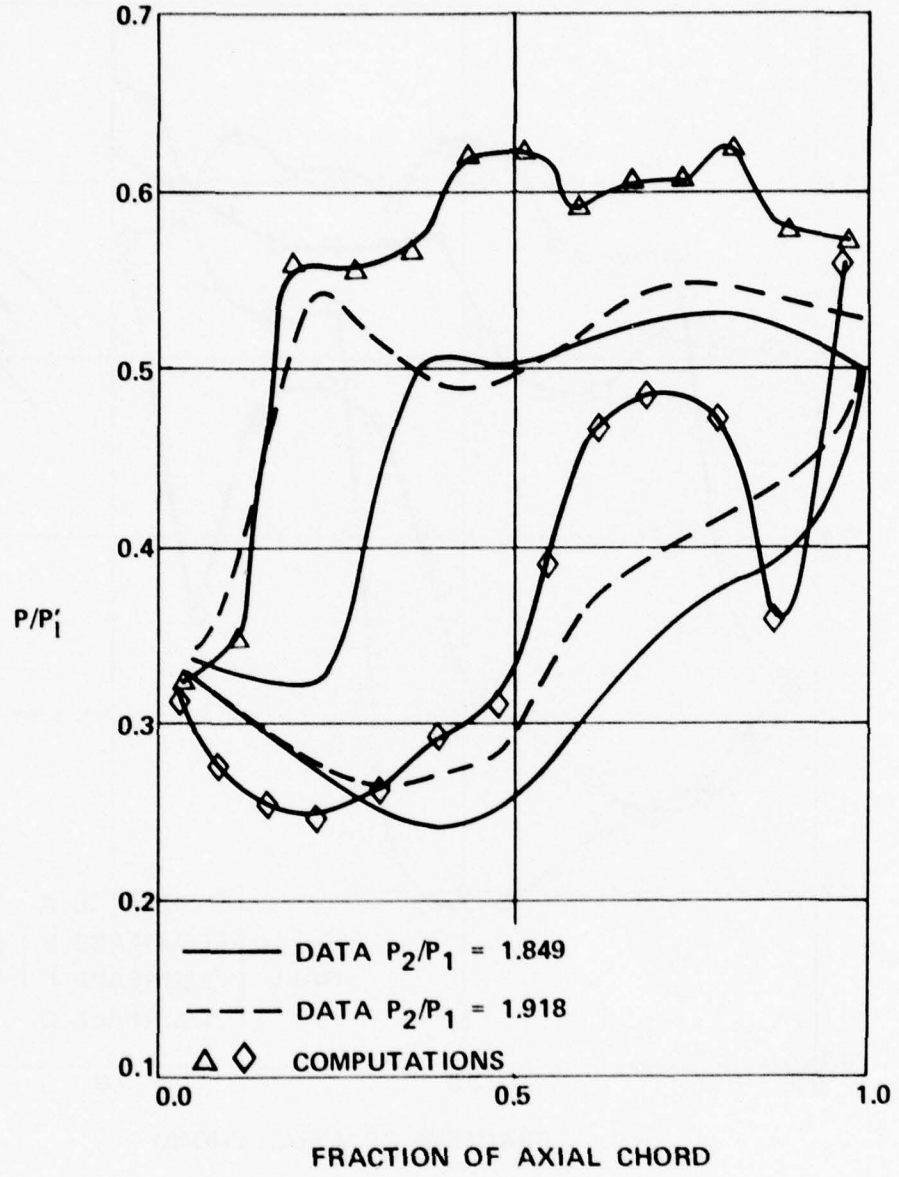

Figure 14. Comparison of Data and Center Blade Calculations, VKI Low Camber DCA Blade

with the leading edge regions reproduced better. Principal regions of disagreement are in the exit region--a region dominated by viscous effects.

ARL Cascade

The ARL cascade has been tested in two forms. The first was without a splitter tested by Holtman et al[14], and the second was with splitters by Holtman et al[9]. A detailed study utilizing a two-dimensional transonic relaxation method, described by Dodge[1], has already been reported. Results agreed well with the data. However, viscous effects had to be modeled by reducing the normal stream tube convergence (b-width). This is required since the calculation technique is inviscid. The result was that the real performance map of the cascade could not be matched because it was throttled. The effect of this deficiency is shown in Figure 15, plotting axial-velocity/density ratio versus exit Mach number. To close exit loading properly, the correct axial-velocity/density ratio must be selected. However, to reasonably match surface loadings, the exit Mach number must be duplicated. These two quantities are far apart for this cascade when an inviscid technique is utilized. The application of the current method alleviates this problem. Results are shown in Figure 16 for surface static-pressure distribution.

Two significant differences between experiment and calculation appear. A compression on the suction surface followed by an acceleration with a near-trailing-edge compression is predicted but not evidenced in the data, or in any of the calculations of Dodge[1]. The origin of this phenomenon is not yet clear. However, it is associated with the high loading of the splittered cascade, since it disappears with the lower-loaded splittered cascade. A Prandtl-Meyer expansion with 20 degrees of turning would produce such an acceleration, while the turning on the suction surface over the same range is 35 degrees. However, it would be unlikely to occur in a test because of the separation after the first compression, and it may not have appeared in earlier calculations because of the lack of three-dimensionality of previous tests. A complete contour map of the suction surface is shown in Figure 17.

The other discrepancy is well documented. A similar but smaller accelerative peak occurs on the pressure surface near the leading edge. Dodge[10] extensively studied this phenomenon, and came to the conclusion that it was due to pressure surface curvature, alternating between expansive at the very leading edge and compressive further down. Figure 18, reproduced from Dodge[10], shows that the pressure surface crosses over in the vicinity of 20 to 30 percent of chord. This effect persists through all calculations by all techniques, and thus must be considered to be real. However, it does not appear in data due to rapid boundary-layer thickening.

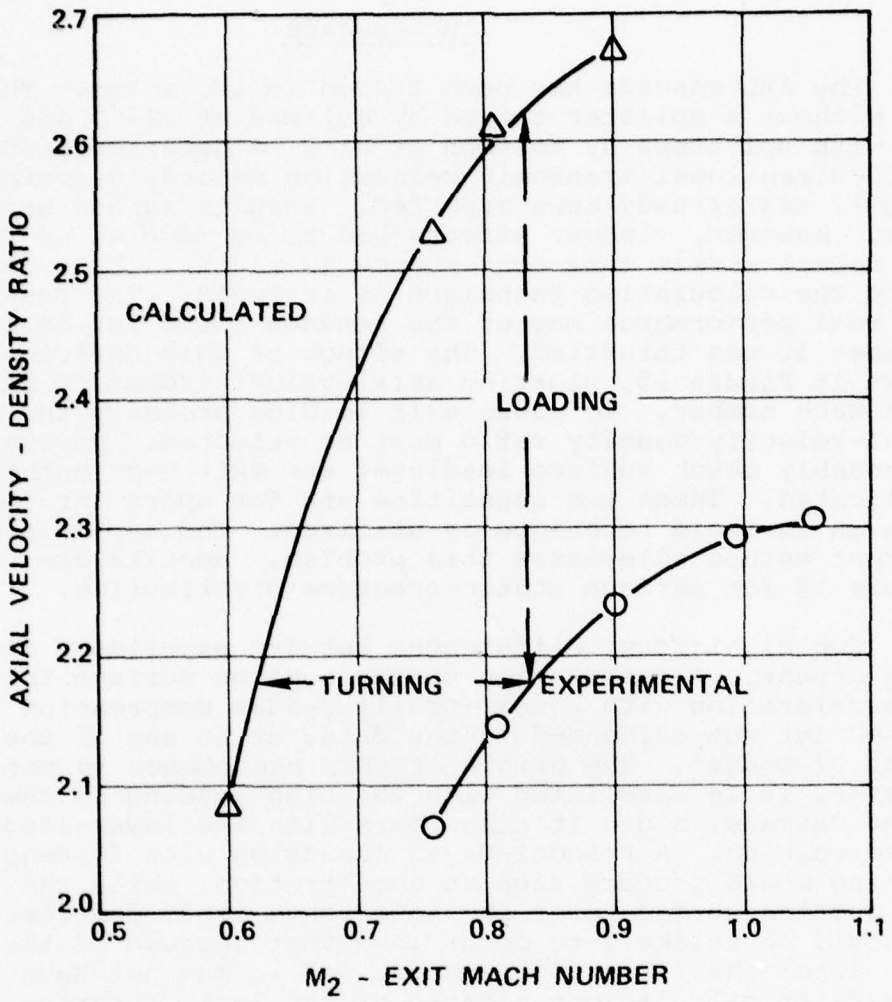

Figure 15. Inviscid Simulation of Real Fluid Conditions in a Cascade

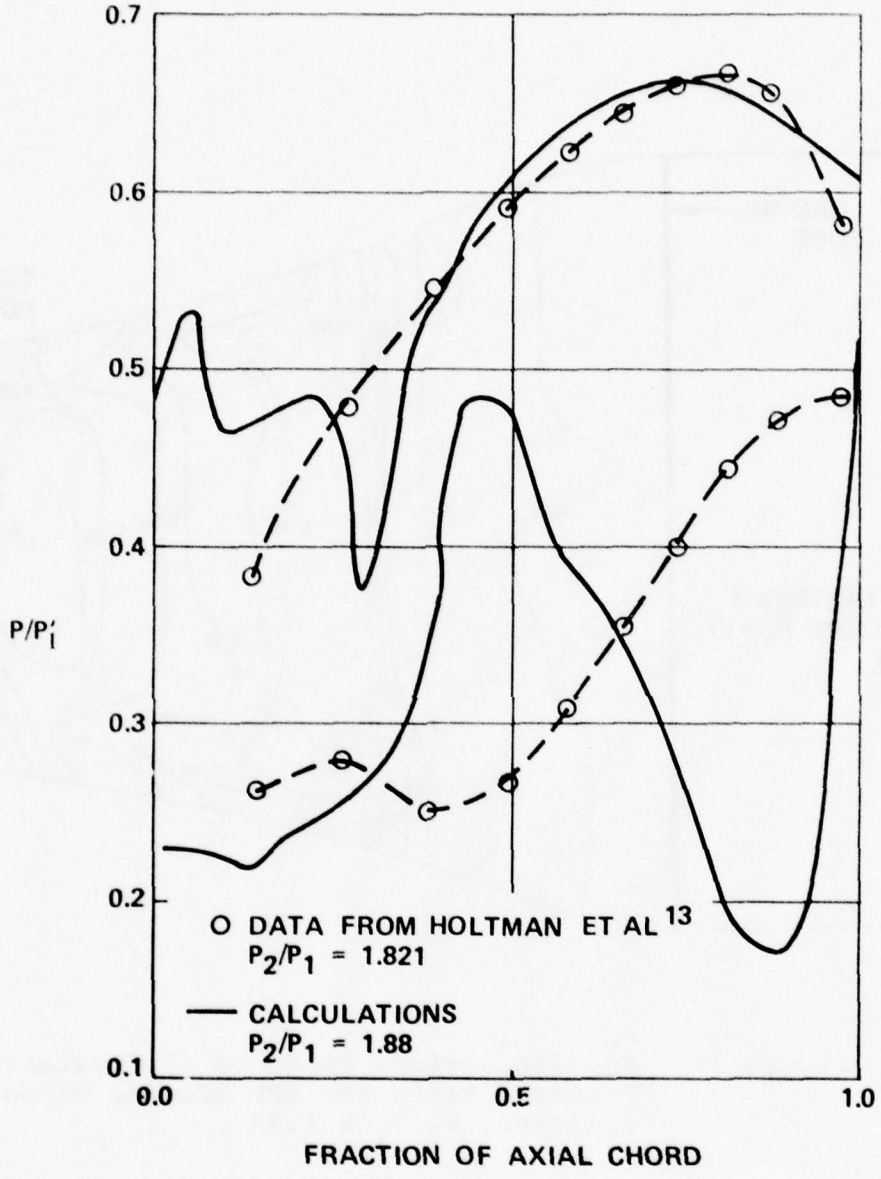

Figure 16. Comparison of Surface Static Pressure Ratio Versus Fraction of Chord for ARL Cascade Without Splitter

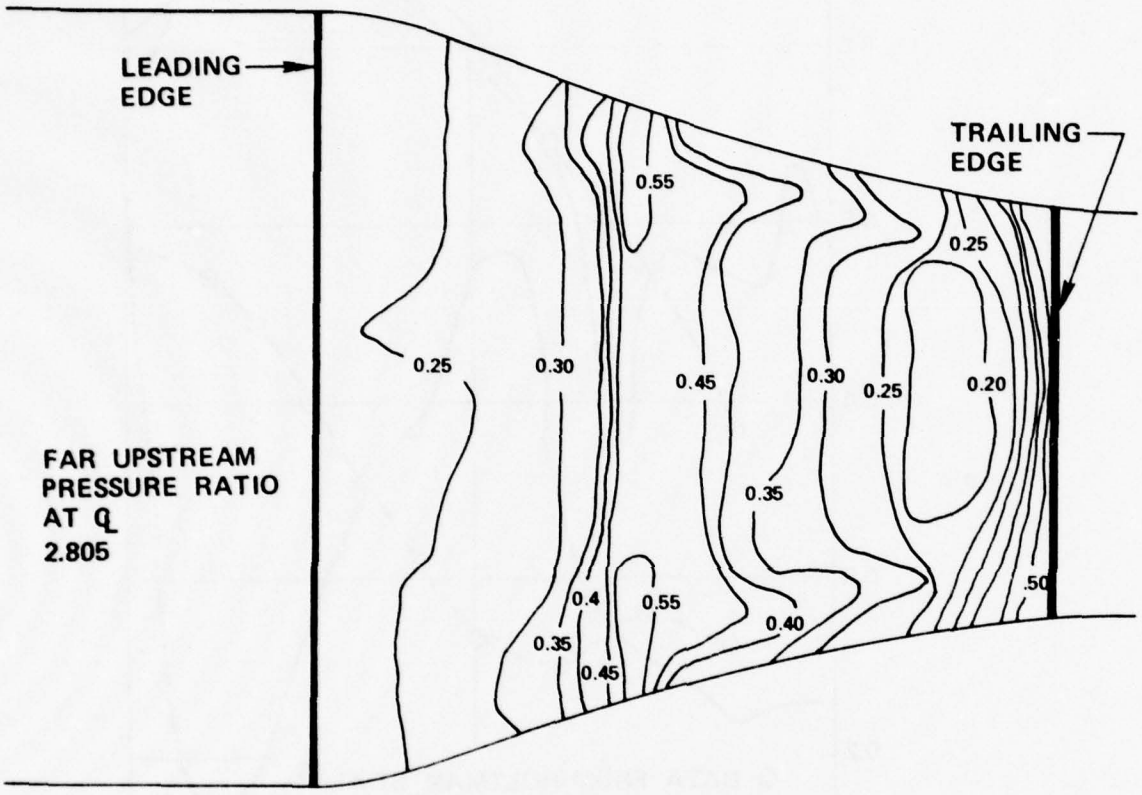

Figure 17. Suction Surface Contours of Constant Static Pressure Ratio for ARL Cascade Without Splitter, $P_2/P_1 = 1.88$

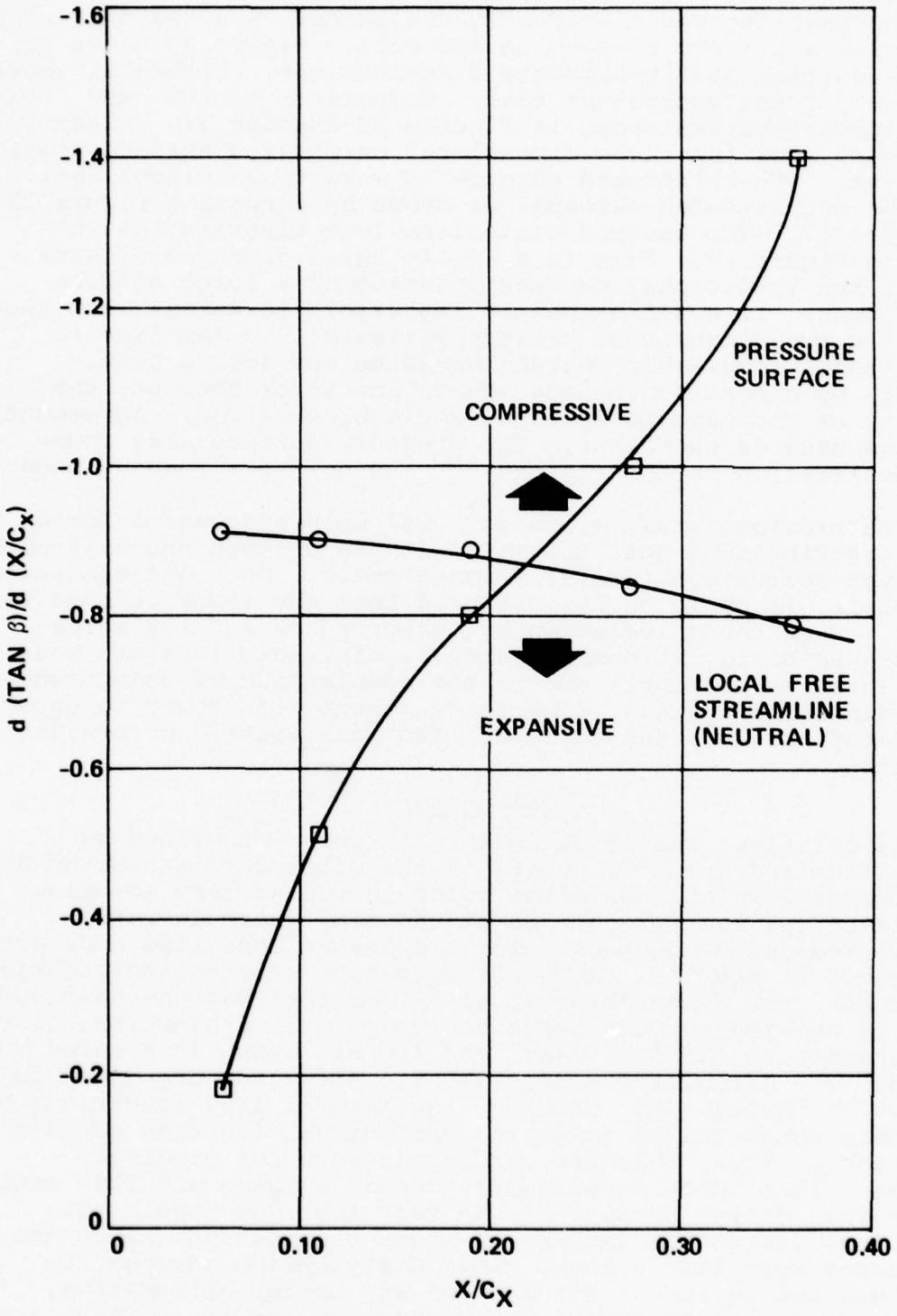

Figure 13. Derivative of Pressure Surface Angle Versus Axial Position

Figure 19 shows the blade shape of the splittered cascade. Like the unsplittered cascade, it was tested as a two-dimensional blade with a sharply converging end wall. Figure 20 shows calculated surface static-pressure distributions. Figure 21 shows the data for the equivalent case. Comparison between the data and calculations are shown in Figures 22 through 24. Figures 25 through 28 show the three-dimensional calculated surface static pressures. The splittered cascade is more three-dimensional than the unsplittered cascade, as shown by comparing Figure 25 to Figure 17. The assumed centerline loss distribution is shown in Figure 29. This is a highly three-dimensional case without the traditional cascade practice of a large uniform center span. It would be nearly impossible to assess what the effective two-dimensional b-width variation, so familiar to conventional compressor design, would be for such a case. However, by comparison to the equivalent rotor section, the validity of the cascade approach would be verified. Agreement with the data is excellent. The pressure surface also shows the acceleration in the vicinity of the splitter leading edge.

The previous study by Dodge[10] was only successful for b-width distributions near the metal (those without end-wall boundary-layer corrections) rate of convergence. On a one-dimensional area basis, it could be demonstrated that the lower passage was choked. When the calculation is performed on a fully three-dimensional basis, as demonstrated herein, solutions are possible. This is apparently due to the combination of using two three-dimensional areas, flow readjustment from lower to upper splittered passage, and the specified loss instead of b-width reduction.

ARL Rotor

Calculations were made on the ARL rotor described by Wennerstrom and Frost[11]. Tests on the rotor were inhibited by a stator choke, which caused the rotor to run at very low flow. The effect was most pronounced at the tip, where deviation angles exceeded 30 degrees. Total pressure loss also approached 50 percent at the tip. Boundary conditions for the calculation were taken from Wennerstrom et al[12], for the through-the-blade match to the 100-percent speed design point. Projections of the grid systems at the hub, mean, and tip are shown in Figures 30 through 32. Calculated surface static pressures are shown in Figures 33 through 36. At high flow angles, flow conditions are extremely sensitive to inlet and exit stream-function boundary conditions. Thus, the exit conditions were not precisely matched. Inlet Mach numbers are generally lower and flow angles higher than design because of the very low flow condition. Conditions are not as extreme as might be expected, since the tip passes very little flow. Loss distribution through the blade was set to linear for lack of any better alternative. This leads to relatively high pressures at the tip. These are probably not realized in the experiment due to very large near-leading-edge total-pressure losses. Blade sections

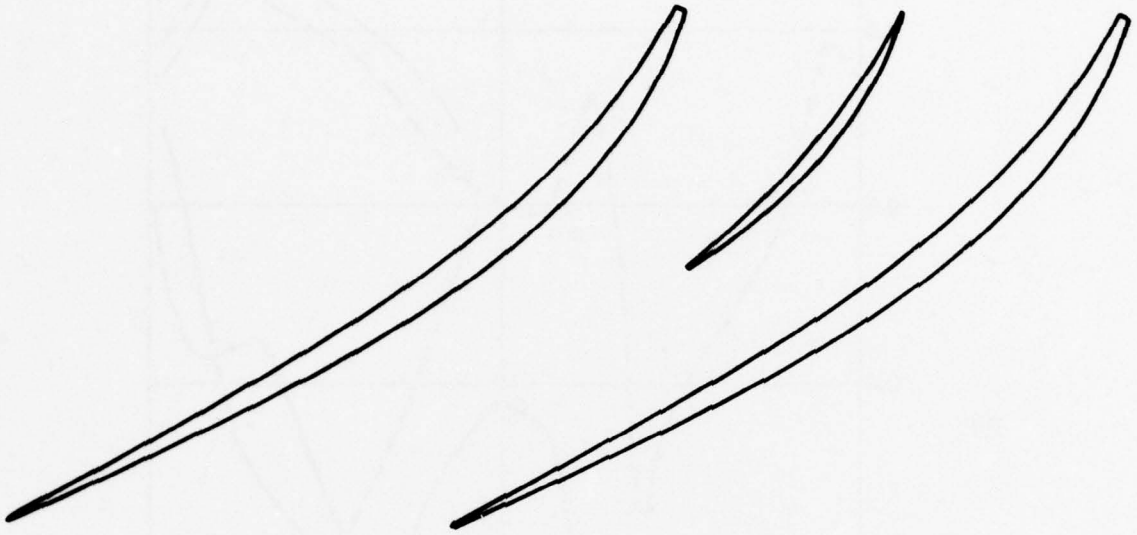

Figure 19. Blade With Splitter Configuration

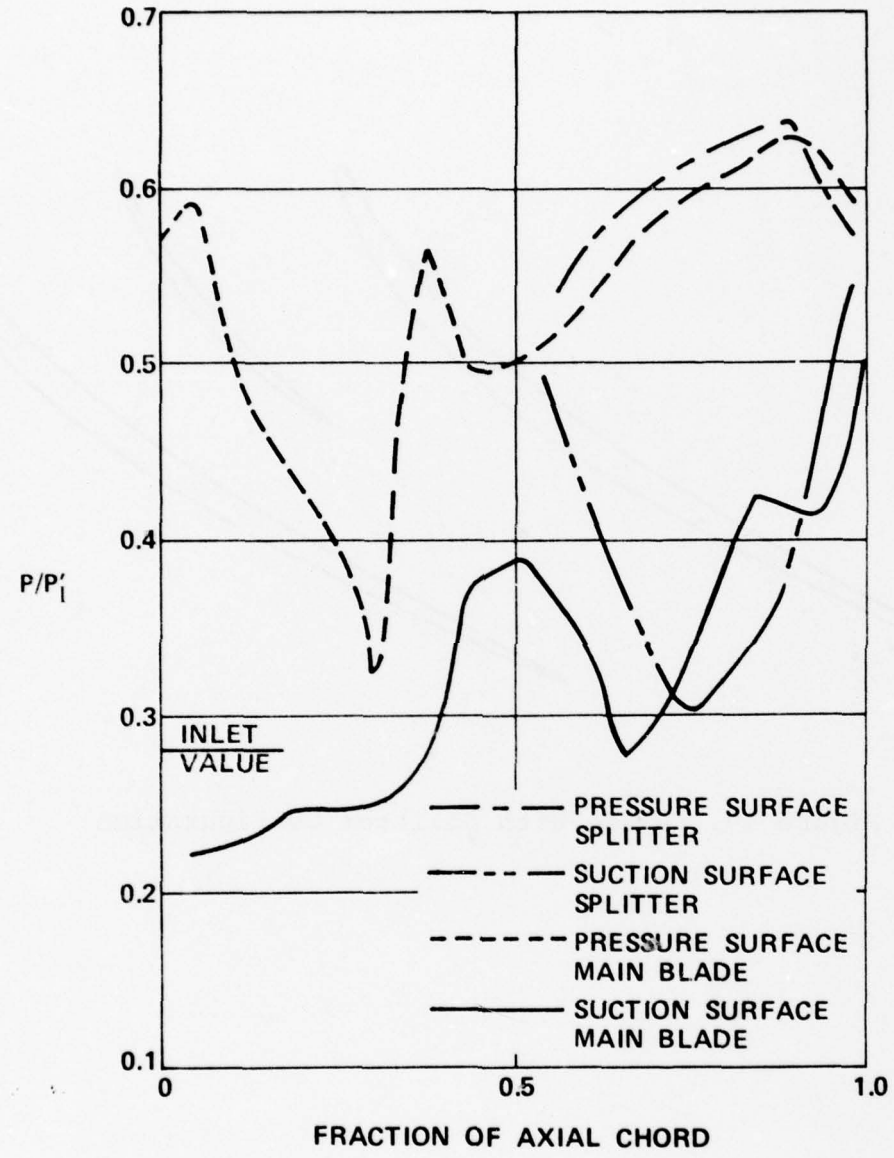

Figure 20. Calculated Surface Static Pressure Distribution, $P_2/P_1 = 1.88$

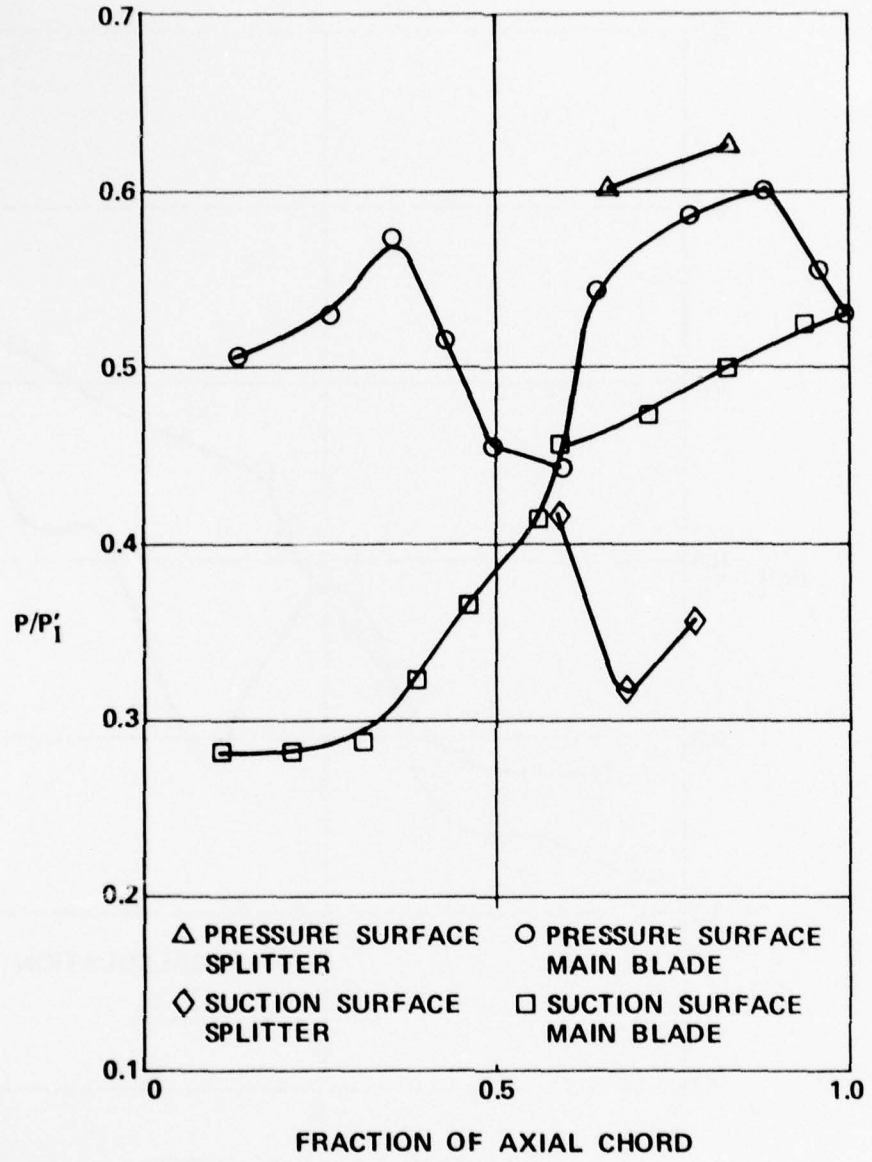

Figure 21. Experimental Data, P_2/P_1 = 1.883

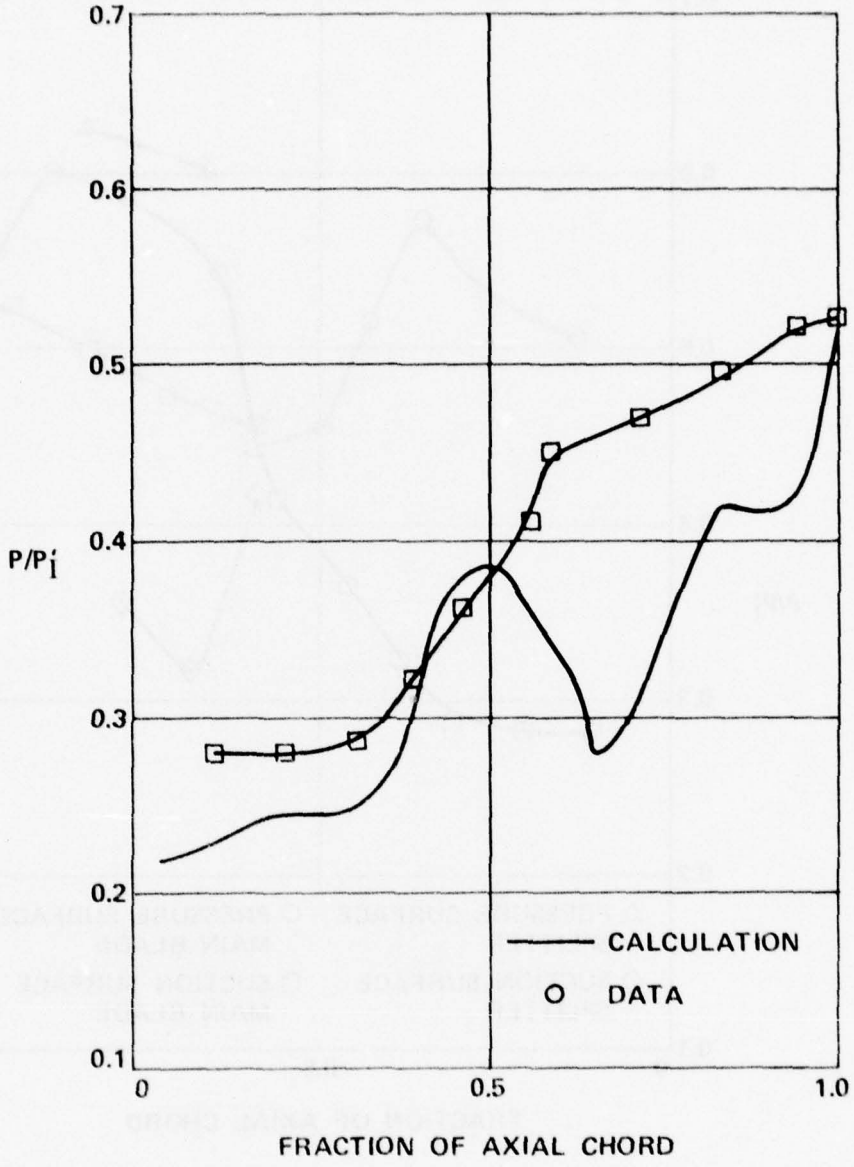

Figure 22. Main Blade Suction Surface Static Pressure Distribution, $P_2/P_1 = 1.88$

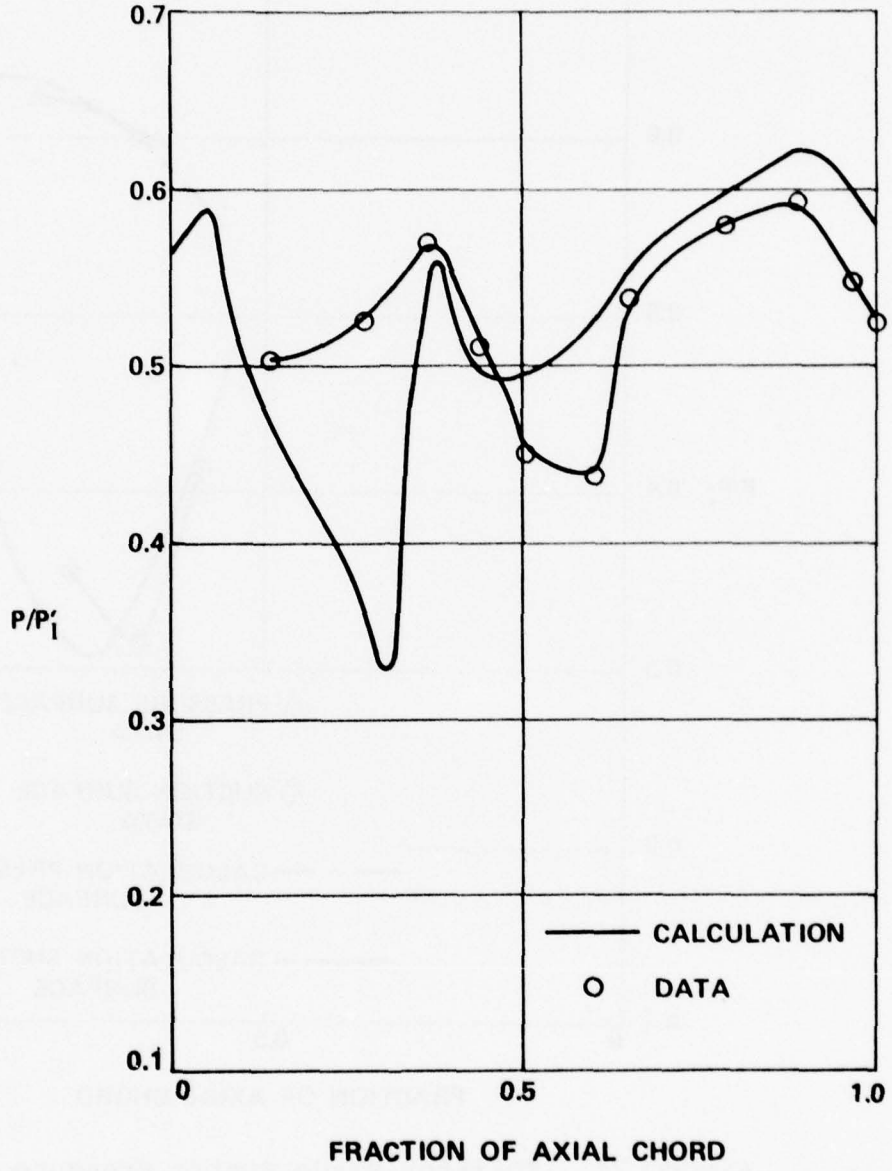

Figure 23. Main Blade Pressure Surface Static Pressure Distribution, $P_2/P_1 = 1.88$

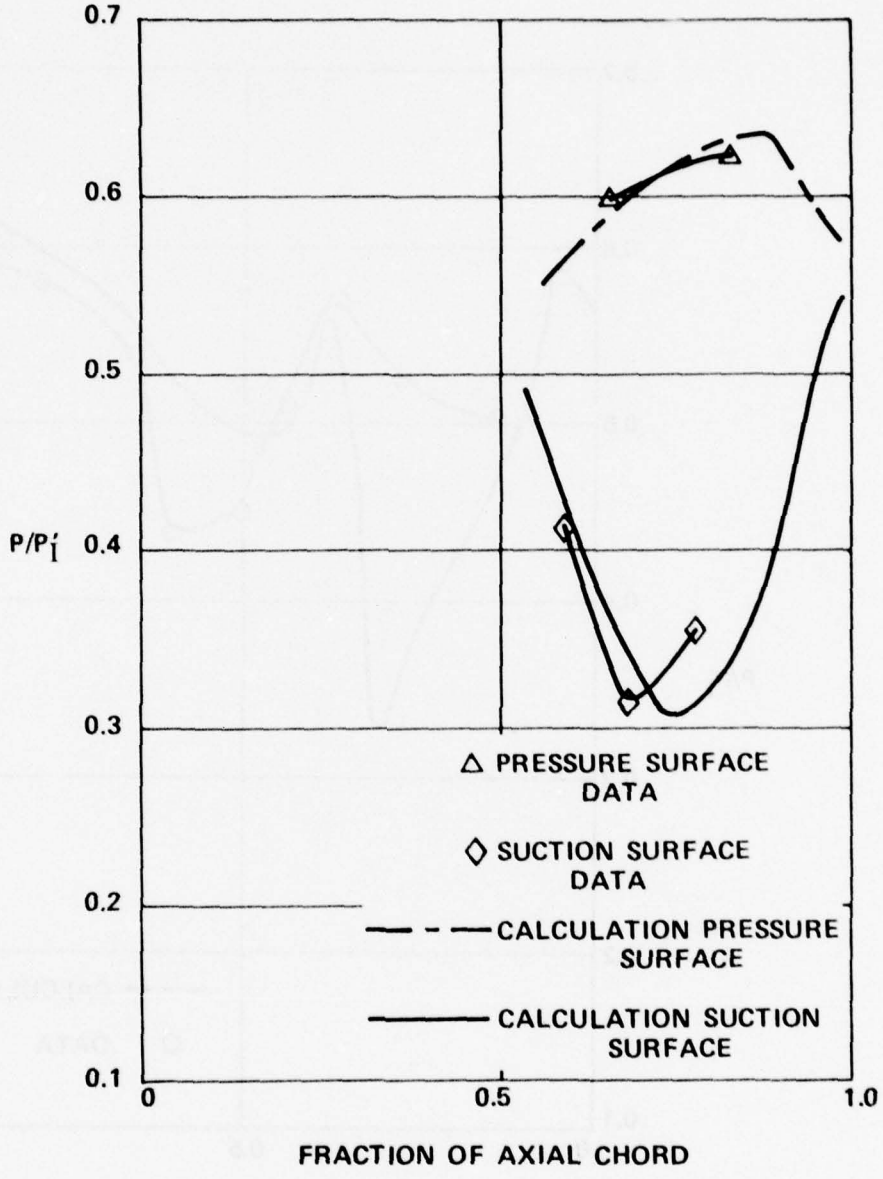

Figure 24. Splitter Blade Static Pressure Distribution, $P_2/P_1 = 1.88$

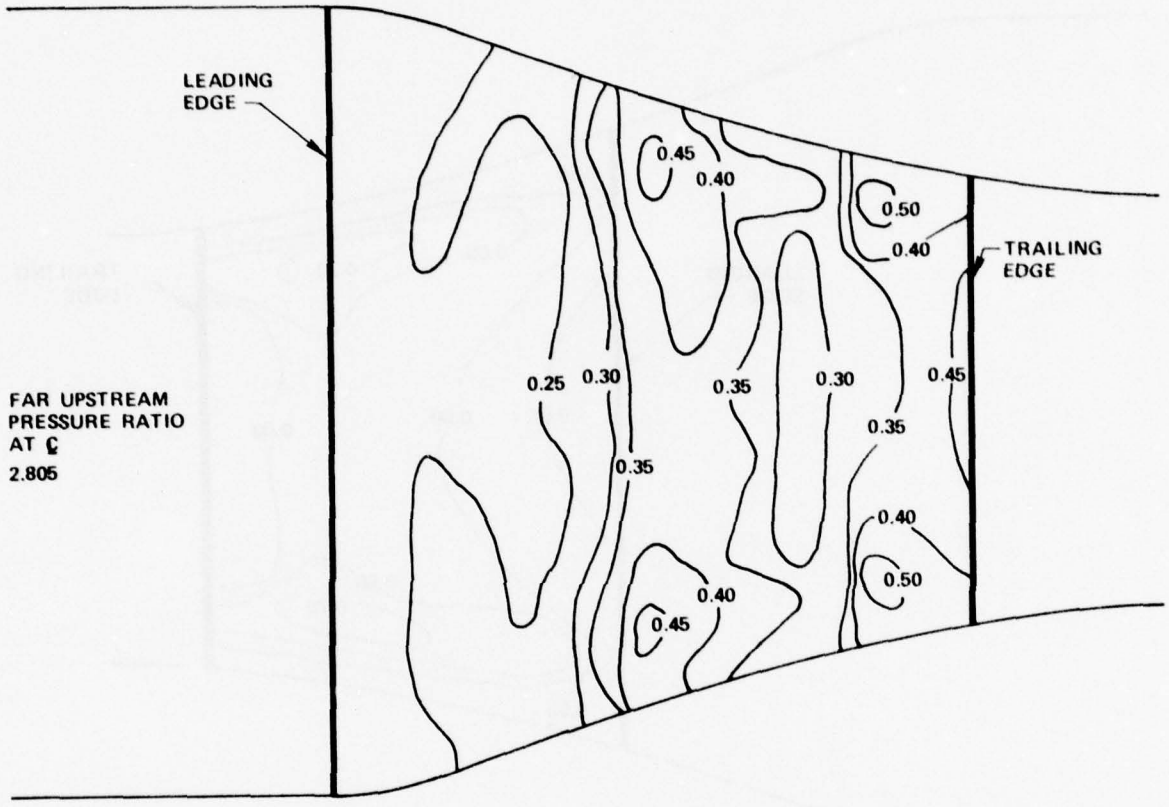

Figure 25. Suction Surface Contours of Constant Static Pressure Ratio for ARL Cascade, $P_2/P_1 = 1.88$

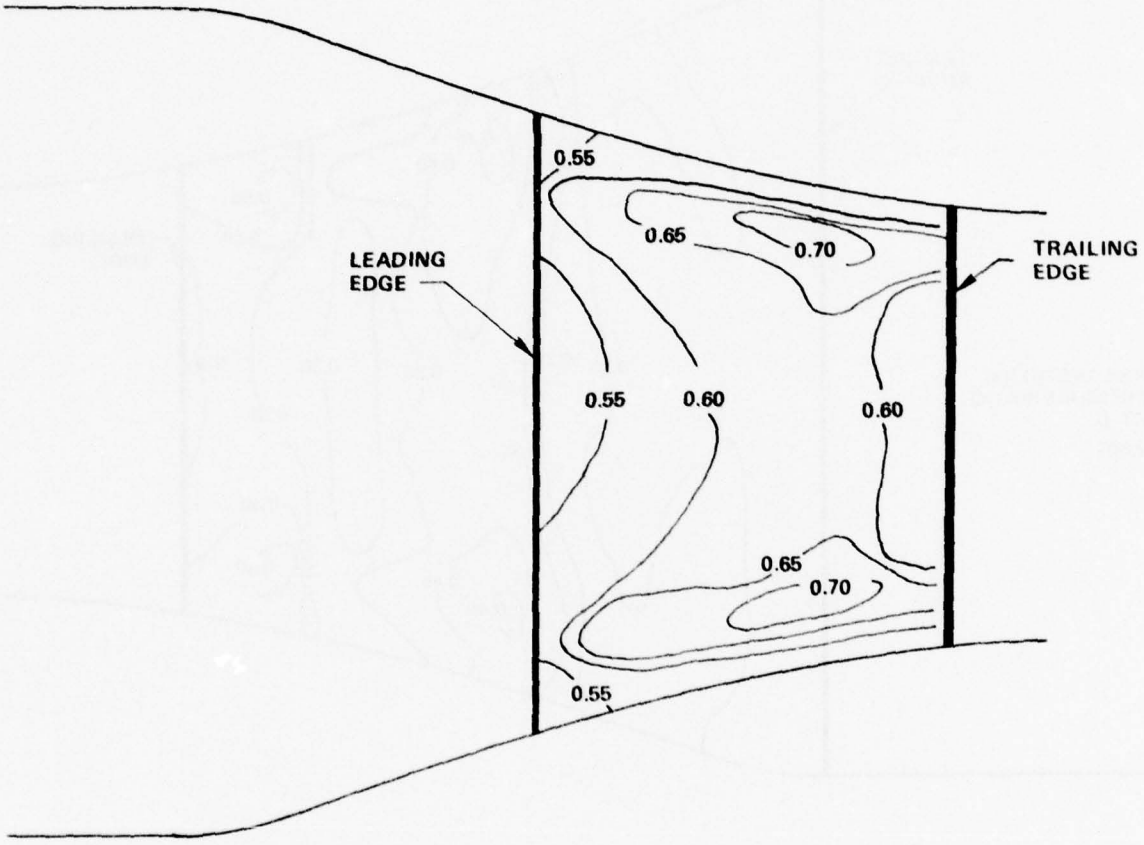

Figure 26. Pressure Surface Contours of Constant Static Pressure Ratio for ARL Cascade with Splitter $P_2/P_1 = 1.88$

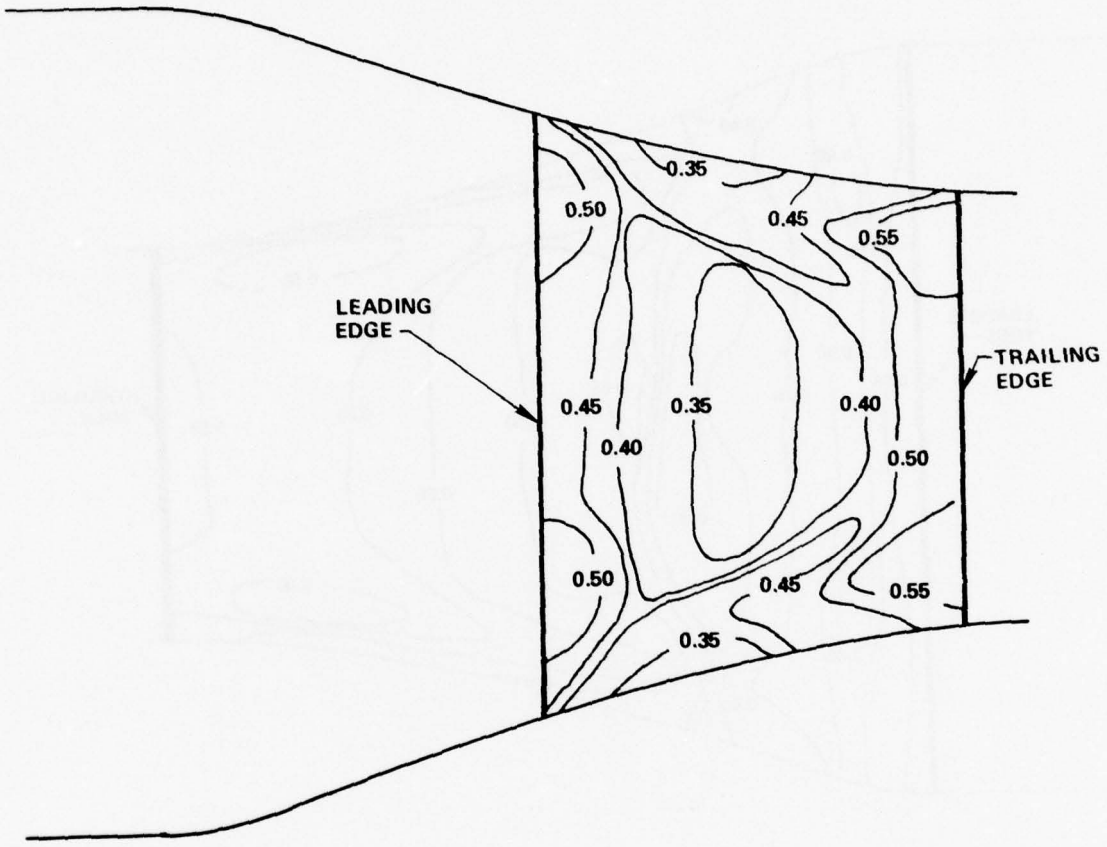

Figure 27. Suction Surface Contours of Constant Static Pressure Ratio for ARL Cascade with Splitter, $P_2/P_1 = 1.88$

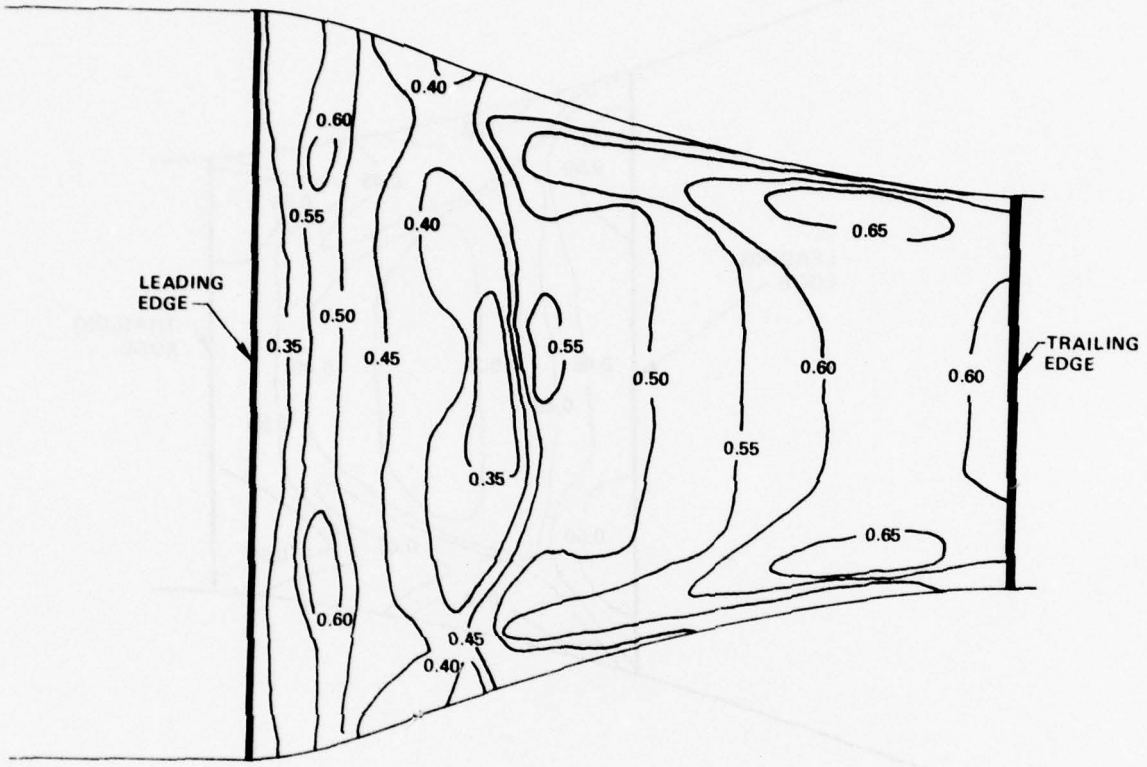

Figure 28. Pressure Surface Contours of Constant Static Pressure Ratio for ARL Cascade, $P_2/P_1 = 1.88$

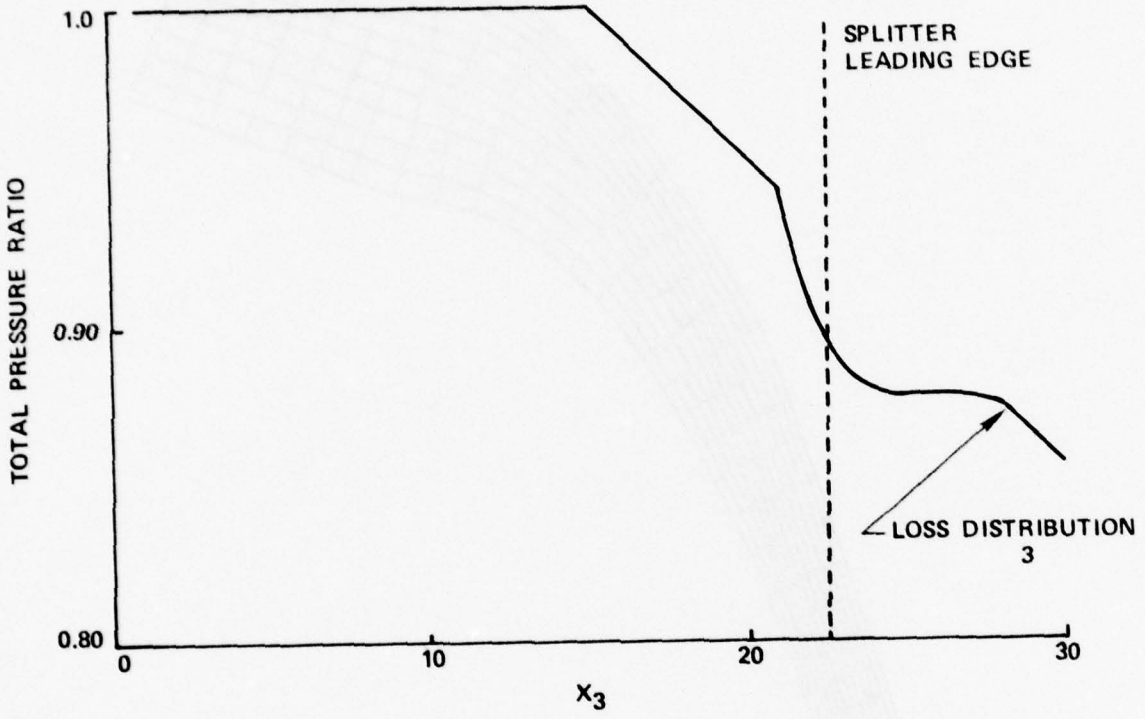

Figure 29. Mid-Span Loss Distribution

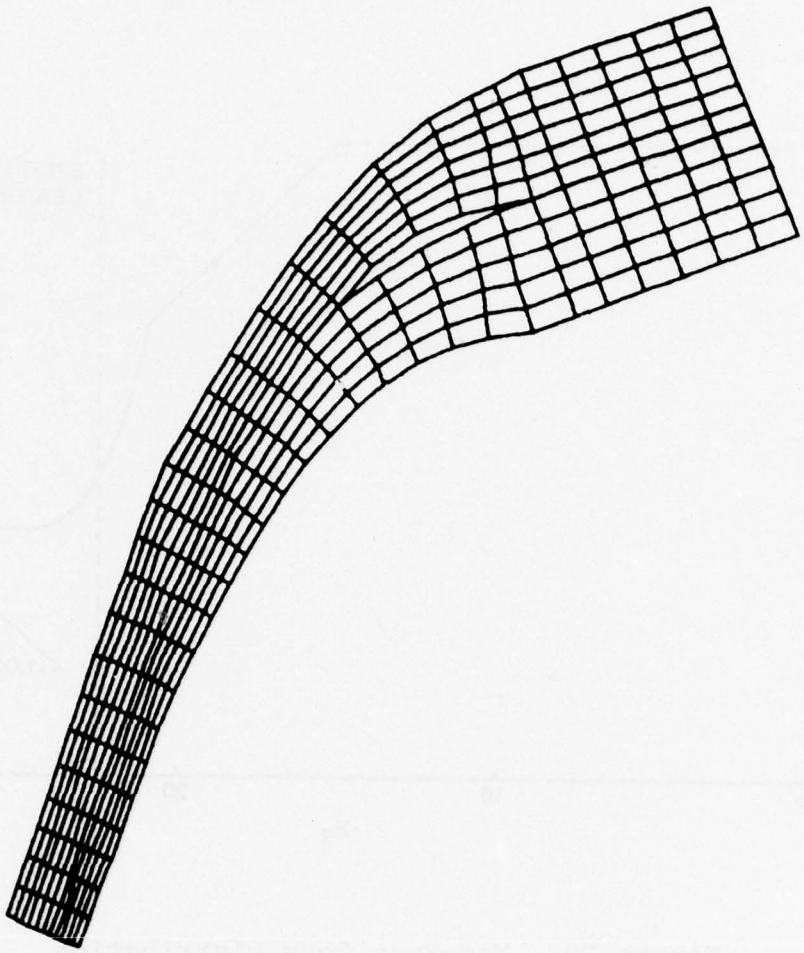

Figure 30. Hub Grid System for ARL Rotor

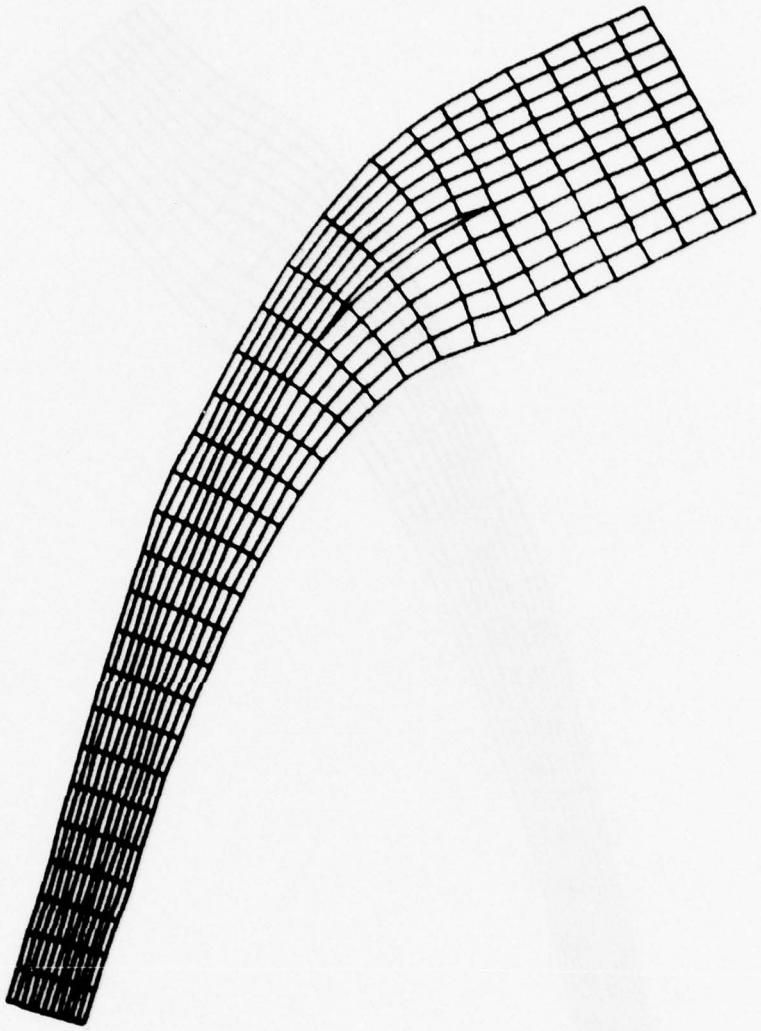

Figure 31. Mean Grid System for ARL Rotor

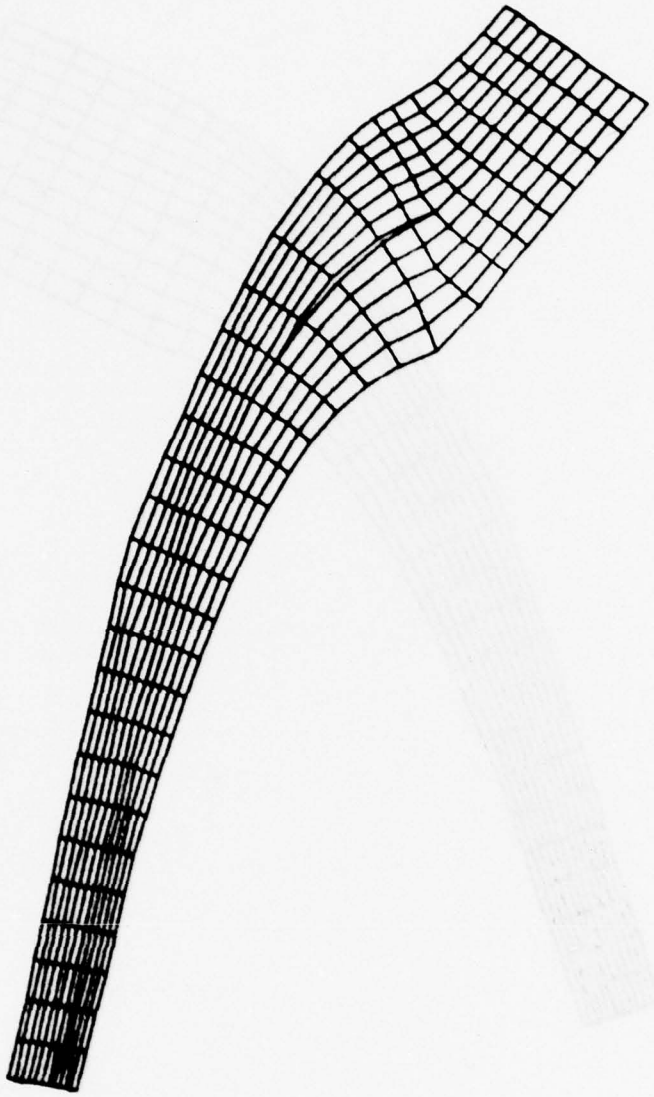

Figure 32. Tip Grid System for ARL Rotor

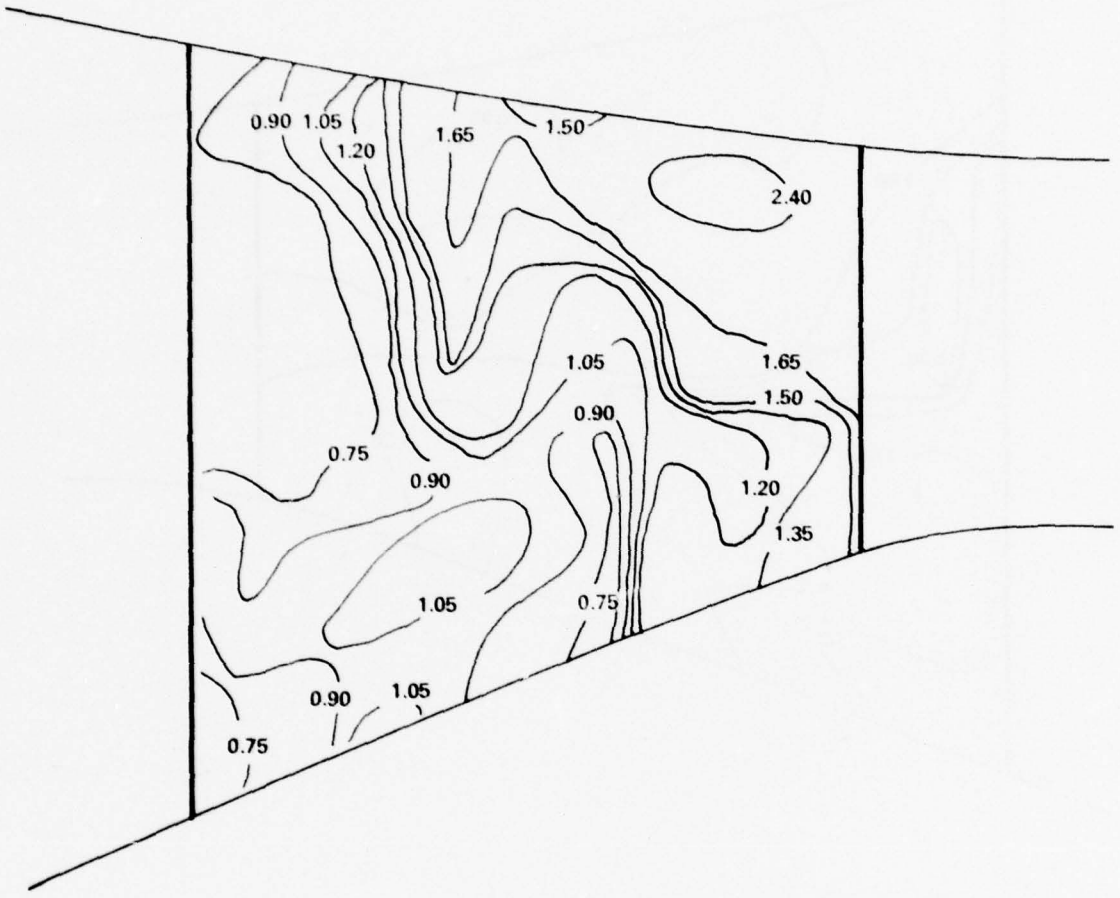

Figure 33. Suction Surface Ratio of Static Pressure to Inlet Total Pressure for ARL Rotor, 100-Percent Design Speed

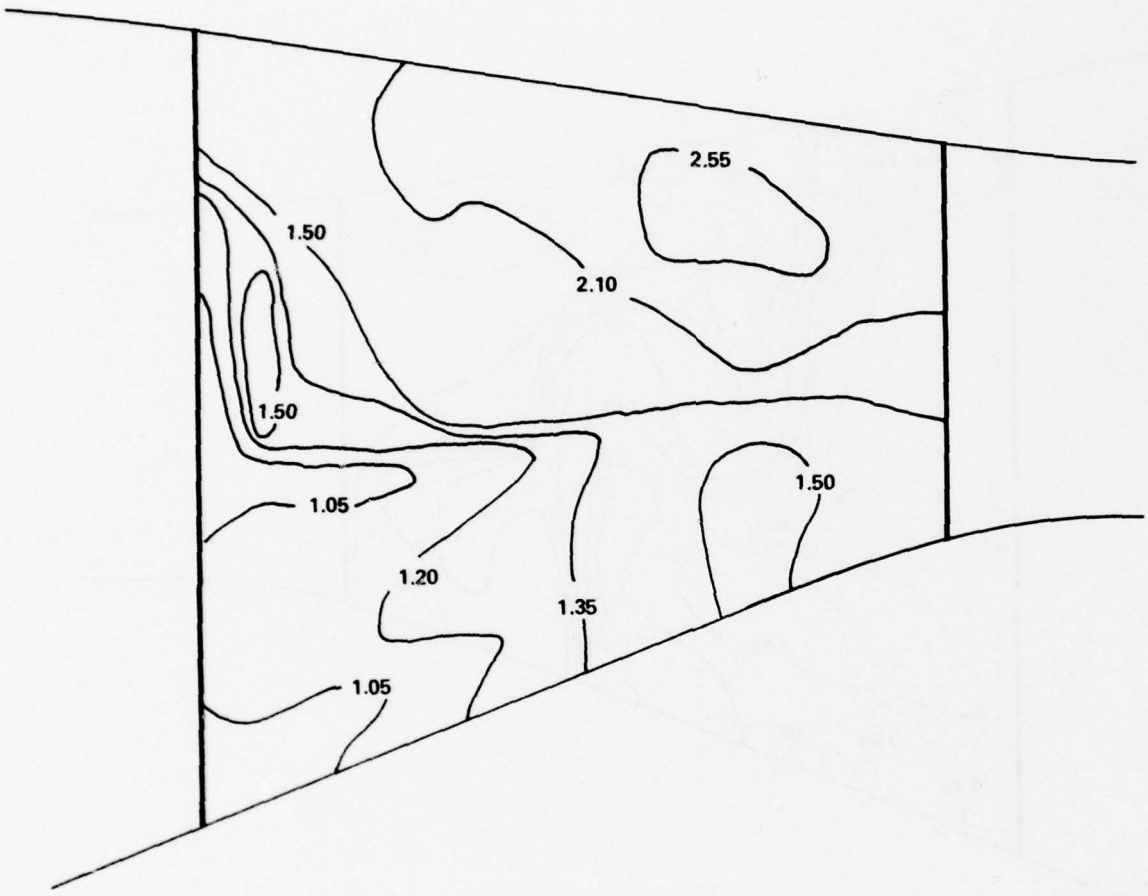

Figure 34. Pressure Surface Ratio of Static Pressure to Inlet Total Pressure for ARL Rotor, 100-Percent Design Speed

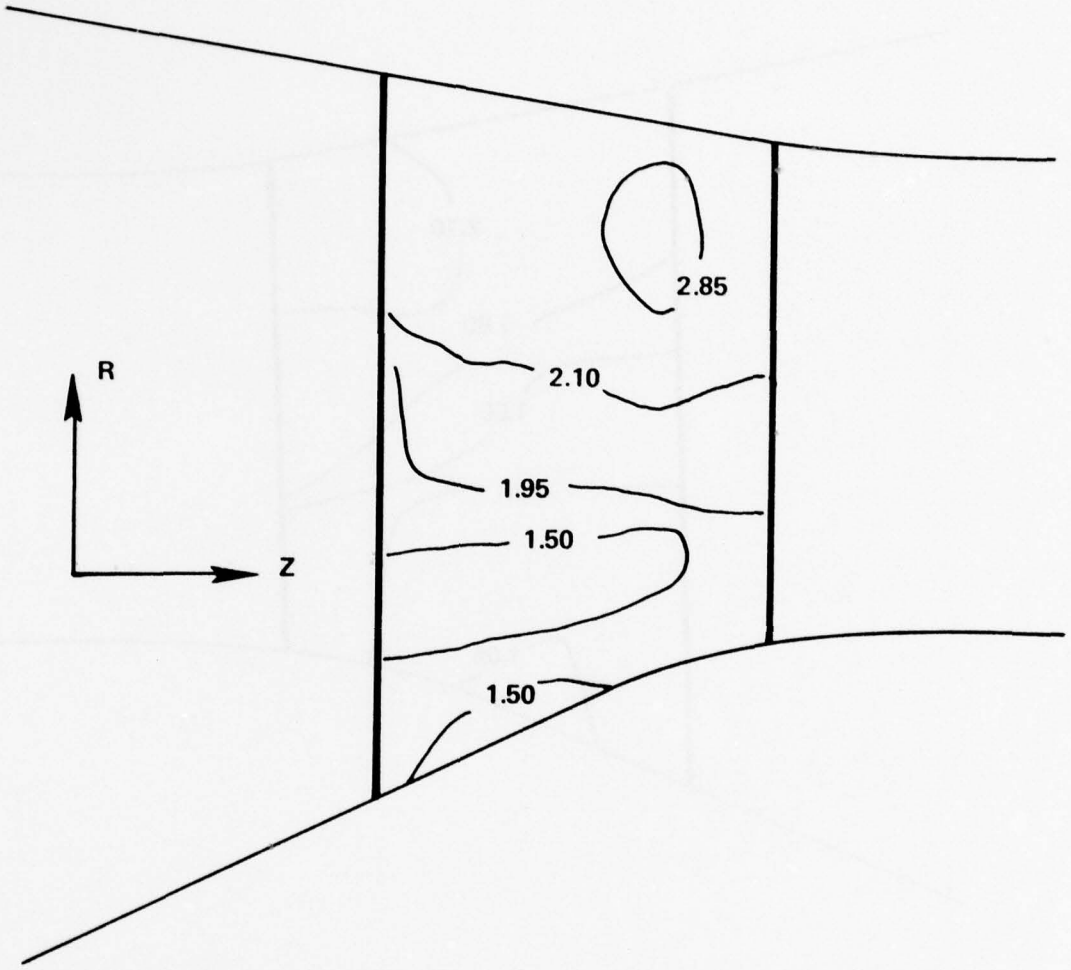

Figure 35. Pressure Surface Ratio of Static Pressure to Inlet Total Pressure for ARL Rotor with Splitter, 100-Percent Design Speed

Figure 36. Suction Surface Ratio of Static Pressure to Inlet Total Pressure for ARL Rotor with Splitter, 100-Percent Design Speed

generally possess an expansion near the leading edge, raising suction surface Mach numbers to design or above. Direct comparison was made to the mid-line section, since it was the one modeled in cascade testing. These surface loadings are shown in Figure 37. Note that suction-surface static pressures are as low as the cascade, despite the lower Mach number upstream (1.34 rotor to 1.46 cascade).

The exit static pressure is slightly higher than reported for the experiment. Rather than rerun the calculation of the rotor, a cascade calculation already available at the higher static pressure was used. The results are shown in Figure 38. The comparison between the rotor and experiment is shown for the main blades in Figure 39, and for the splitter in Figure 40. The agreement is excellent, providing strong evidence that the cascade was a good simulation to the center section of the rotor. This fact was already somewhat experimentally confirmed by comparing rotor cascade loss coefficients.

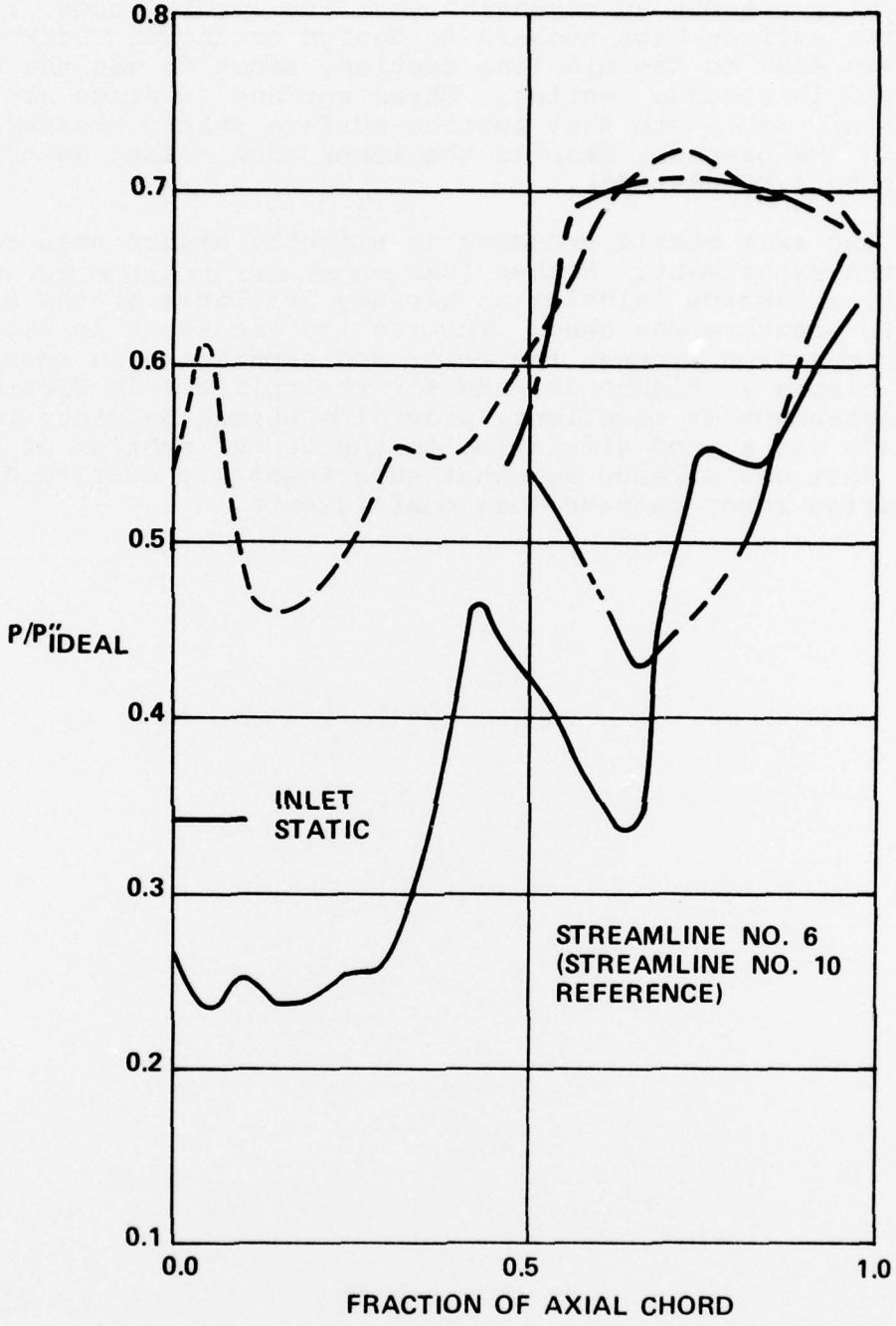

Figure 37. Ratio of Static Pressure to Local Ideal Relative Total Pressure Versus Fraction of Axial Chord for ARL Rotor

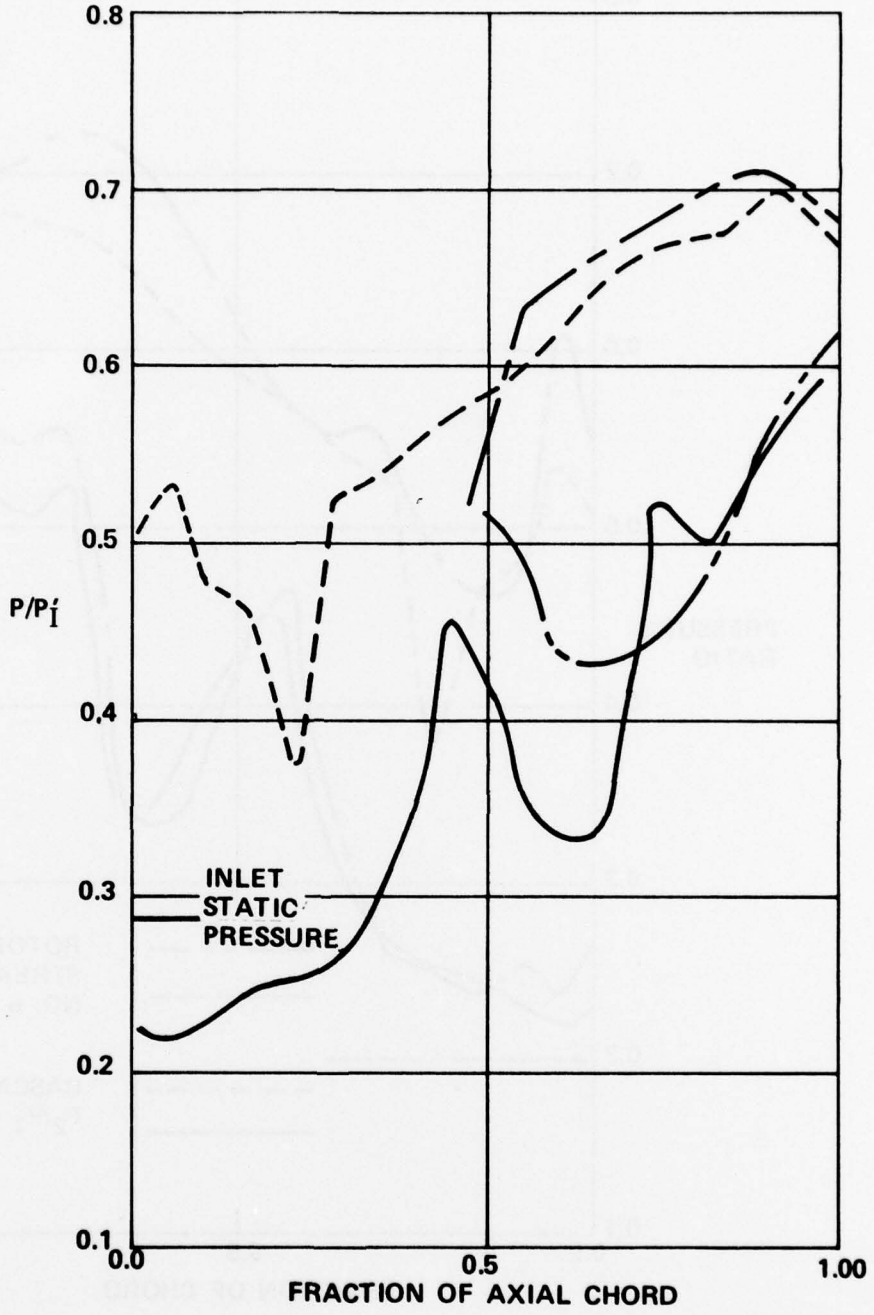

Figure 38. Ratio of Static Pressure to Inlet Total Pressure for ARL Cascade, $P_2/P_1 = 2.36$

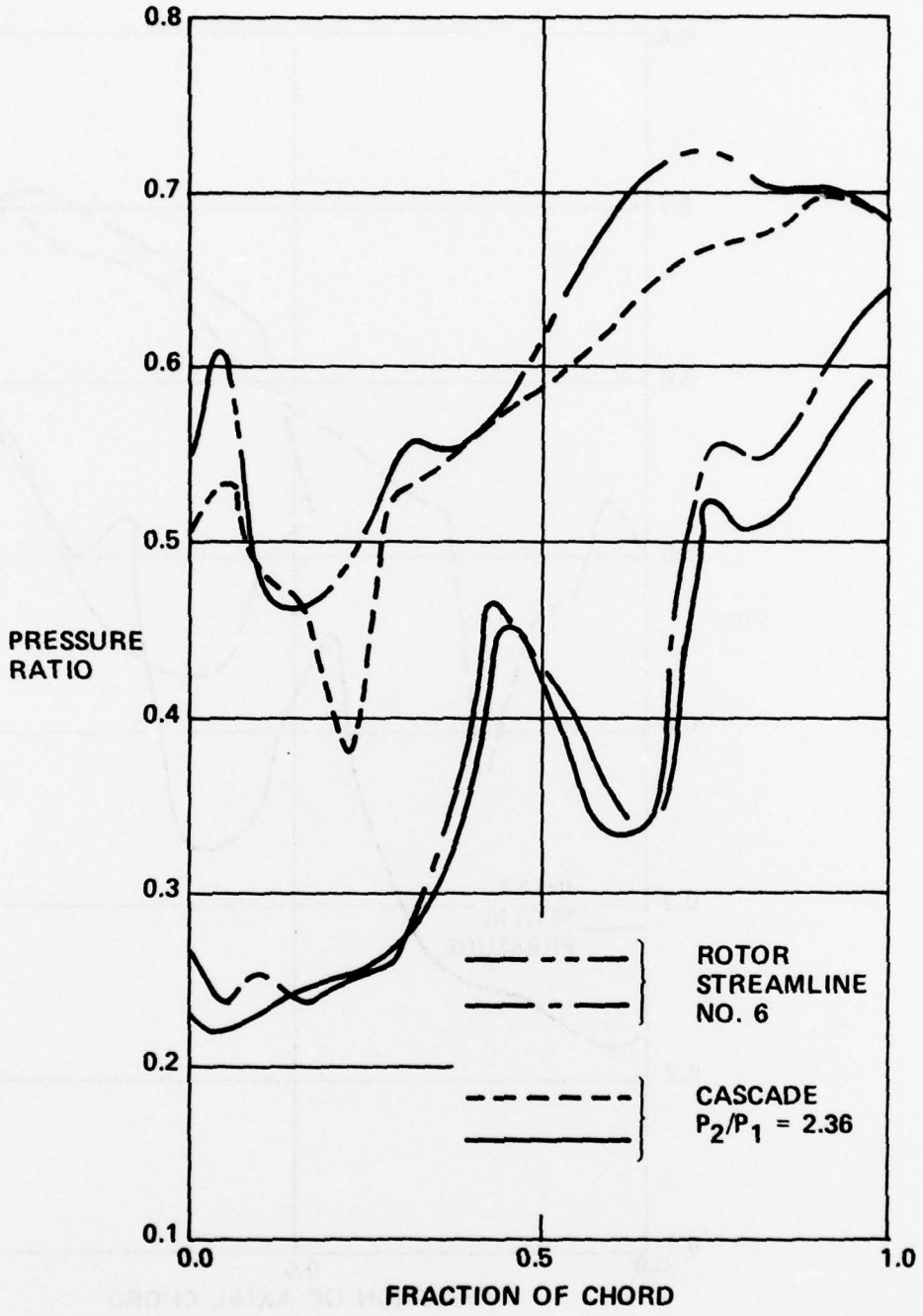

Figure 39. Comparison of Main Blade Static Pressures Between Cascade and Rotor Mean Section

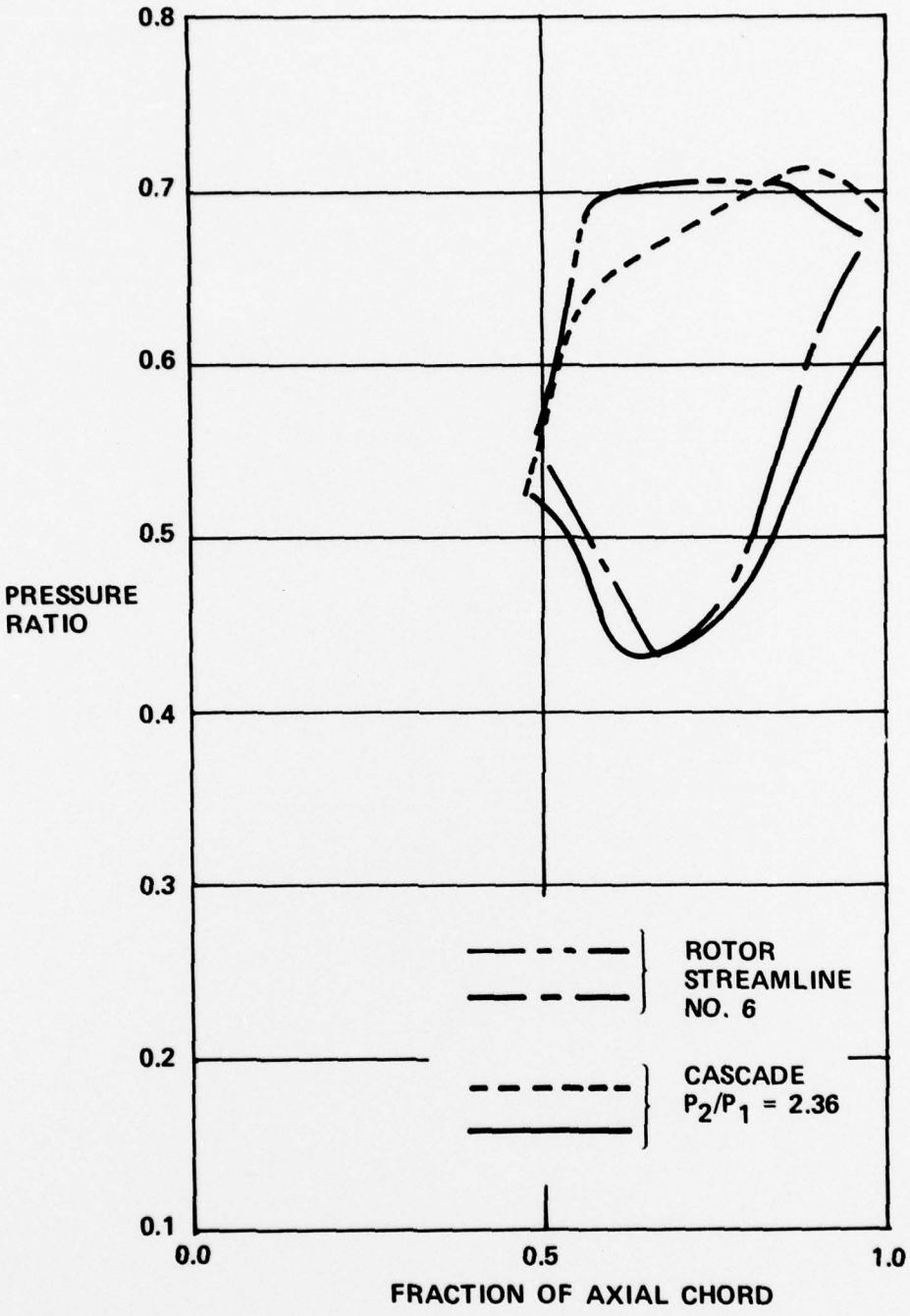

Figure 40. Comparison of Splitter Blade Static Pressure Between Cascade and Rotor Mean Section

SECTION IV

CONCLUSIONS AND RECOMMENDATIONS

The most significant conclusion from this study is that a technique has been developed, coded, and to limited degree verified offering substantial insight into the three-dimensional flow fields internal to compressors. Moreover, this computer code is a practical design tool. Run times range from 10 to 12 minutes on the CDC 174 (1.0 to 1.2 minutes on the CDC 7600). Input is arranged so that almost any conceivable compressor configuration can be handled, including multiple splitters of varying shape and extent.

Comparison between the calculation and the splittered cascade tested by ARL is excellent. When the calculation is applied to the rotor, the section that corresponds to the cascade in shape and overall construction has almost precisely the same predicted static pressure distribution as the cascade prediction. This suggests that the cascade is reasonably representative of the rotor section. A word of caution. This conclusion only applies to this particular section through this particular rotor. This section was carefully selected by the designers to have minimum three-dimensional effects. Other sections and other rotors need to be examined on a case by case basis, which is now possible with this new numerical method.

The close agreement between computation and experiment tends to support the concept of a supersonic inlet cascade with sharply coverging end walls. The end wall has a powerful effect on the flow distribution; however, the centerline results indicate reasonable simulation of stream-tube convergence is present in the rotor. Again, care must be exercised against over generalizing this conclusion. Each new case needs to be examined on its own merits.

Several years of intensive development of massive numerical computer simulations to internal flow devices has shown that performance may be strongly affected by choices of the traditional overall parameters; such as solidity, aspect ratio, diffusion ratio, etc. However, after these parameters are optimized to a particular application, the designer still faces many decisions on the final blade shape. These choices are not trivial. They can and do affect performance substantially; in some cases, a great deal more than do the traditional parameters. Without internal-flow visibility, total optimization is not possible. In the case of turbine stators, where significant differences in surface static pressure are not as likely to occur, internal-flow visibility must take the form of completely viscous solutions. However, a brief perusal of any high Mach number compressor, such as the one shown herein, indicates significant regions of unwanted diffusion. Much better performance could be obtained by eliminating such diffusion. This

study presents the method to predict and thereby eliminate unnecessary diffusion. The ultimate test should now be experimental. An extensive optimization of a stage with already good performance will indicate what the final payoff in design of this numerical method will be.

REFERENCES

1. Dodge, P.R., "A Non-Orthogonal Numerical Method for Solving Transonic Cascade Flows," ASME Paper 76-GT-63.

2. Dodge, P.R., "Transonic Relaxation Methods," Transonic Flow Problems in Turbomachinery, edited by T.C. Adamson and M.F. Platzer, Hemisphere Publishing Co., Washington, 1977.

3. Rae, W.J., "Finite-Difference Calculations of Three-Dimensional Transonic Flow Through a Compressor Blade, Using the Small-Disturbance Non-Linear Potential Equation," Transonic Flow Problems in Turbomachinery, edited by T.C. Adamson and M.F. Platzer, Hemisphere Publishing Co., Washington, 1977.

4. Rae, W.J., "Calculations of Three-Dimensional Transonic Compressor Flow Fields by a Relaxation Method," AIAA Paper 77-199.

5. Tompkins, W.T. and D.A. Oliver, "Through Flow Calculations in Axial Turbomachinery," presented at the 47th PED meeting.

6. Dodge, P.R., "A Numerical Method for 2-D and 3-D Viscous Flows," AIAA Journal, Volume 15, pp 961-965, July 1977.

7. Wu, C.H., "A General Theory of Three-Dimensional Turbomachines of Axial, Radial, and Mixed Flow Types," NACA TN 2604.

8. Owczarek, J.A., "Fundamentals of Gas Dynamics," International Textbook Company, Scranton, PA., 1964.

9. Holtman, R.L., R.B. McClure, and G.T. Sinnet, "Test of a Supersonic Compressor Cascade with Splitter Vanes", ARL Report 73-0142, December 1973.

10. Dodge, P.R., "Transonic Two-Dimensional Flow Analysis of Compressor Cascade with Splitter Vanes," AFAPL Report AFAPL-TR-75-110, December 1975.

11. Wennerstrom, A.J. and G.R. Frost, "Design of a Rotor Incorporating Splitter Vanes for a High Pressure Ratio Supersonic Axial Compressor Stage," ARL 74-0110, August 1974.

12. Wennerstrom, A.J., W.A. Buzzell, and R.D. DeRose, "Test of a Supersonic Axial Compressor Stage Incorporating Splitter Vanes in the Rotor," ARL 75-0165, AD A014732, June 1975.

13. Breugelmans, F.A.E. and H. Starken, "The Cascade and Rotor Section Performance of a 9.57° Cambered DCA Airfoil," presented at von Karman Institute for Fluid Dynamics Lecture Series 59, May, 1973.

14. Holtman, R.L., G.D. Huffman, R.B. McClure, and G.T. Sinnet, "Test of a Supersonic Compressor Cascade (Vol. I)," ARL 72-0170, Vol I, December 1972.

15. Murman, E.M. and J.D. Cole, "Calculation of Plane Steady Transonic Flows," AIAA paper 70-188, 1970.

APPENDIX A

RELAXATION METHOD

The major extension of the current program over that reported earlier by Dodge[6] is in the relaxation area. Since the discovery of transonic relaxation techniques by Murman and Cole[15], the technique for solving Equation (31) has been available. Since that time, much has been learned about this technique. No attempt to discuss relaxation processes in detail is contained herein. Rather, an explanation of what is in the current program and a brief discussion of why, follows.

In its simplest form, Murman's method provides a consistent approach for solving Equation (A-1).

$$(1-M^2)\frac{\partial^2\phi}{\partial s^2} + \frac{\partial^2\phi}{\partial n^2} = \alpha\frac{\partial^2\phi}{\partial s^2} + \frac{\partial^2\phi}{\partial n^2} = 0. \qquad \text{(A-1)}$$

When M^2 is less than unity, Equation (A-1) is elliptic. Ordinary centered differences result in a relaxation process essentially equivalent to that used in the incompressible program. When M is greater than one, the equation becomes hyperbolic, and the region of influence changes to that contained by a set of characteristics. To model this, differences must be switched to backward at the sonic point. For supersonic flow, the difference Equation (A-2) was given by Murman and Cole[15].

$$\frac{\alpha}{\Delta s^2}\left(\phi_{i,j} - 2\,\phi_{i-1,j} + \phi_{i-2,j}\right) + \frac{1}{\Delta n^2}\left(\phi_{i,j+1} - 2\,\phi_{i,j} + \phi_{i,j-1}\right) = 0. \qquad \text{(A-2)}$$

where $s = s_o + i\Delta s$

$n = n_o + j\Delta n$

If the difference solution for potential is assumed to be a continuous function, it can be expanded by a Taylor's series about $\phi_{i,j}$. When this is done and substituted into Equation (A-2), Equation (A-3) results.

$$(M^2-1)\left\{\frac{\partial^2\phi}{\partial s^2} + \sum_{k=3}^{\infty}\frac{1}{k!}\frac{\partial^k\phi}{\partial s^k}\left[2^k - 2\right](-1)^k\,\Delta s^{k-2}\right\} = \frac{\partial^2\phi}{\partial n^2} + \sum_{k=3}^{\infty}\frac{1}{k!}\frac{\partial^k\phi}{\partial n^k}\left[1 + (-1)^k\right]\Delta n^{k-2} \qquad \text{(A-3)}$$

---

[15] Murman, E.M. and Cole, J.D., "Calculation of Plane Steady Transonic Flows", AIAA Paper 70-188, 1970.

Note that the equation is consistent. The lowest order truncation is then given by Equation (A-4).

$$T_3 = - (M^2-1) \frac{\partial^3 \phi}{\partial s^3} \Delta s \qquad \text{(A-4)}$$

In the conventional sense, this difference is first order in s. Note, however, that the magnitude of truncation error increases with Mach number. At unity, when the difference equation and the differential equation match regions of influence exactly, the system is second order.

Dodge[1] suggested a nonorthogonal method that was second order, and matched precisely regions of influence. In a fixed grid this method can be applied in an approximate fashion. Consider the difference Equation (A-5).

$$D = \phi_{i,j} - \phi_{i-1,j+1} - \phi_{i-1,j-1} + \phi_{i-2,j} \qquad \text{(A-5)}$$

The equivalent partial differential equation to Equation (A-5) is given by Equation (A-6).

$$D = \sum_{k=1}^{\infty} \left\{ \frac{1}{k!} \frac{\partial^k \phi}{\partial s^k} (-1)^k (2^k-2) \Delta s^k - \sum_{r=0}^{k-1} \frac{1}{r!m!} \frac{\partial^k \phi}{\partial s^r \partial n^m} (-\Delta s)^r (\Delta n)^m (1 + (-1)^m) \right\} \qquad \text{(A-6)}$$

where $m + r = k$

The first few terms of this series are given by Equation (A-7).

$$\frac{D_o}{\Delta s^2} = \frac{\partial^2 \phi}{\partial s^2} - \frac{\Delta n^2}{\Delta s^2} \frac{\partial^2 \phi}{\partial n^2} - \Delta s \frac{\partial}{\partial s} \left[\frac{\partial^2 \phi}{\partial s^2} - \frac{\Delta n^2}{\Delta s^2} \frac{\partial^2 \phi}{\partial n^2} \right] + \ldots = 0. \qquad \text{(A-7)}$$

---

[1] Dodge, P.R., "A Nonorthogonal Numerical Method for Solving Transonic Cascade Flows", ASME Paper 76-GT-63.

If Equation (A-8) holds, then Equation (A-7), and thereby Equation (A-5), are second-order consistent approximations to Equation (A-1).

$$\frac{\Delta s^2}{\Delta n^2} = M^2 - 1 \tag{A-8}$$

At this point, the characteristics of the differential equation and difference equation match precisely, as indicated below.

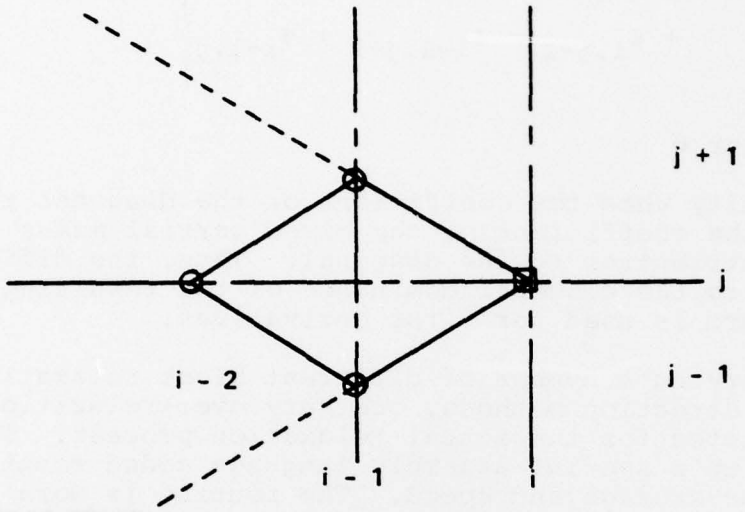

CHARACTERISTICS

However, this is only a consistent approximation when Equation (A-8) applies. An approximation that is second-order when M is unity and when Equation (A-8) holds, and first-order in between, is given by Equation (A-9).

$$\frac{\partial^2 \phi}{\partial s^2} = \frac{1}{\Delta s^2}\left\{\phi_{i,j} - \phi_{i-1,\,j+1} - \phi_{i-1,j-1} + \phi_{i-2,j}\right\} + \frac{1}{\Delta s^2}\left\{\phi_{i,j+1} - 2\phi_{i,j} + \phi_{i,j-1}\right\} \tag{A-9}$$

Substitution of Equation (A-9) into Equation (A-1) results in a consistent approximation.

In the full 3-D case, first derivatives and mixed second partials must also be considered. Instead of using centered differences, the following are used:

$$\frac{\partial^2 \phi}{\partial X^*_1 \partial X^*_2} = \frac{\delta}{2}\Big\{\phi_{i+1,j+1} - \phi_{i,j+1} - \phi_{i+1,j} + 2\phi_{i,j} - \phi_{i-1,j} - \phi_{i,j-1} + \phi_{i-1,j-1}\Big\} + \frac{(1-\delta)}{2}\Big\{\phi_{i+1,j} - 2\phi_{i,j} - \phi_{i+1,j-1} + \phi_{i-1,j-1} + \phi_{i,j+1} - \phi_{i-1,j+1} + \phi_{i-1,j}\Big\}$$

where $\delta = 1$ or 0

δ is unity when the coefficient of the diagonal terms divided by the coefficient of the mixed partial makes an opposite contribution to the diagonal. Thus, the difference contributes to the diagonal dominance of the resulting matrix. A similar form is used for first derivatives.

After trying a number of different block relaxation and alternating direction methods, ordinary over-relaxation was finally selected for the actual relaxation process. This is implemented in a special assembly language coded routine that is optimized for storage and speed. The routine is more than three times faster than the Fortran routine it replaces.

GLOSSARY OF TERMS

A	Area
a	Speed of sound
C	Local wheel speed
$\vec{G}$	Guessed velocity
h	Enthalpy
h'	Total enthalpy
I	Rothalpy
P	Static pressure
P'	Total pressure
R	Gas constant
r	Radius
S	Entropy
T	Temperature
t	Time
$\vec{U}$	Rotational component of velocity
$\vec{W}$	Velocity in the relative plane
z	Axial position
γ	Ratio of specific heats
θ	Angular displacement
λ	Second coefficient of viscosity
μ	Viscosity
ρ	Density
Σ	Shearing stress vector
ϕ	Velocity potential
ω	Rotational frequency

☆U.S.Government Printing Office: 1978 — 757-080/753